

# Radiative transfer and radiative driving of outflows in active galactic nuclei and starbursts

G. S. Novak,<sup>1,2★</sup> J. P. Ostriker<sup>1</sup> and L. Ciotti<sup>3</sup>

<sup>1</sup>*Department of Astrophysical Sciences, Peyton Hall, Princeton University, Princeton, NJ 08544, USA*

<sup>2</sup>*Observatoire de Paris, LERMA, CNRS, 61 Av de l'Observatoire, 75014 Paris, France*

<sup>3</sup>*Department of Astronomy, University of Bologna, via Ranzani 1, I-40127 Bologna, Italy*

Accepted 2012 July 31. Received 2012 July 31; in original form 2012 March 29

## ABSTRACT

To facilitate the study of black hole fuelling, star formation and feedback in galaxies, we outline a method for treating the radial forces on interstellar gas due to absorption of photons by dust grains. The method gives the correct behaviour in all of the relevant limits [dominated by the central point source; dominated by the distributed isotropic source; optically thin; optically thick to ultraviolet (UV)/optical; optically thick to infrared (IR)] and reasonably interpolates between the limits when necessary. The method is explicitly energy conserving so that UV/optical photons that are absorbed are not lost, but are rather redistributed to the IR where they may scatter out of the galaxy. We implement the radiative transfer algorithm in a two-dimensional hydrodynamical code designed to study feedback processes in the context of early-type galaxies. We find that the dynamics and final state of simulations are measurably but only moderately affected by radiative forces on dust, even when assumptions about the dust-to-gas ratio are varied from zero to a value appropriate for the Milky Way. In simulations with high gas densities designed to mimic ultraluminous IR galaxies with a star formation rate of several hundred solar masses per year, dust makes a more substantial contribution to the dynamics and outcome of the simulation. We find that, despite the large opacity of dust to UV radiation, the momentum input to the flow from radiation very rarely exceeds  $L/c$  due to two factors: the low opacity of dust to the re-radiated IR and the tendency for dust to be destroyed by sputtering in hot gas environments. We also develop a simplification of our radiative transfer algorithm that respects the essential physics but is much easier to implement and requires a fraction of the computational cost.

**Key words:** blackhole physics – radiative transfer – methods: numerical – galaxies: active – quasars: general.

## 1 INTRODUCTION

Supermassive black holes (SMBHs) are thought to inhabit the central regions of nearly all massive galaxies and have properties well correlated with those of their host galaxies (Ferrarese & Merritt 2000; Gebhardt et al. 2000; Tremaine et al. 2002; Novak, Faber & Dekel 2006; Gültekin et al. 2009). The direction of the causal link between SMBH and host galaxy properties remains unclear, but the existence of such a correlation implies an intimate connection between the physics of SMBH growth and galaxy formation, spanning a factor of at least  $10^4$  in length scale from  $\sim 1$  pc to  $\sim 10$  kpc.

Quasars came to astronomers' attention due to their enormous electromagnetic output. Bright active galactic nuclei (AGN) emit

as much as  $10^{47}$  erg s<sup>-1</sup> over the electromagnetic spectrum (Woo & Urry 2002; Kollmeier et al. 2006). A significant amount of careful work has been performed to study the physical effects of this extraordinary outpouring of electromagnetic energy and momentum on the material in the immediate vicinity of the AGN (e.g. Proga, Stone & Kallman 2000; Proga, Ostriker & Kurosawa 2008; Kurosawa & Proga 2009; Park & Ricotti 2011, 2012). As a result, we are beginning to understand the radiation-driven broad-line winds emerging from discs around the central SMBHs. However, relatively little work has been done regarding the radiative effects on the surrounding galaxy.

There has been intense theoretical interest in the ability of AGN to affect the star formation histories and observed colours of galaxies (e.g. Croton et al. 2006; Schawinski et al. 2007). The relationships between star formation and AGN activity, galaxy mergers and secular processes have turned out to be complex and the parameter

★E-mail: greg.novak@obspm.fr

space is not yet fully mapped. What is clear is that gas added to the central regions of galaxies will induce a central starburst and an AGN flare-up, but the triggering mechanism remains uncertain.

Although the use of numerical simulations to study the interactions between black holes and galaxies has a long history (e.g. Binney & Tabor 1995; Ciotti & Ostriker 1997), work by Di Matteo, Springel & Hernquist (2005) and Springel, Di Matteo & Hernquist (2005) set off an explosion of theoretical work. They studied the simplest reasonable fully specified model of black hole fuelling and AGN feedback in the context of a major merger of gas-rich spiral galaxies and found that the AGN has a profound effect on the gas dynamics and star formation history in the merger remnant.

During the combined AGN/starburst phase, analytical investigations by Thompson, Quataert & Murray (2005) and Murray, Quataert & Thompson (2005) have shown the importance of radiative forces on dust. Subsequent numerical work (Debuhr et al. 2010; Debuhr, Quataert & Ma 2011, 2012) has verified that if the central  $\simeq 100$  pc of galaxies are assumed to have optical depths of 10–25 in the infrared (IR), due to dust opacity, then radiative forces on dust have dramatic dynamical consequences in the context of merging galaxies.

As the investigations have become more detailed and accurate, it has become increasingly necessary to perform the radiative computations in a more rigorous fashion, carefully determining both the energy and momentum input into the ambient gas. It is the purpose of this paper to outline some of the principles and techniques that may be used for this task.

Our goal is to develop a numerical method to self-consistently solve the radiative transfer problem in galaxies in the presence of dust and radiation produced by stars and AGN. That is, we would like to solve for the specific intensity of the radiation field for a given distribution of radiation sources in the presence of scattering and absorbing media, and subsequently use the specific intensity to compute the forces on the scattering/absorbing media. Studies of SMBH fuelling and AGN feedback performed to date have either ignored radiative effects or assumed a particular form of the photon field which is then used to compute forces on the gas.

Although it would be ideal to obtain a perfect solution for the radiation field in all cases, we will settle for a method that gives the correct asymptotic behaviour in all relevant limits and interpolates reasonably between the limits. It should respect global conservation laws for energy and momentum. It must not be overwhelmingly demanding in terms of algorithmic complexity or computational resources.

The paper is organized as follows. In Section 2, we summarize previous theoretical work on AGN feedback as well as some recent observational results. In Section 3, we discuss the radiative transport equation in the context of the present problem. We describe the physics behind it, its most important properties and the different approaches that can be used for the numerical solution. In Section 4, we describe the physics implemented in a two-dimensional hydrodynamical code designed to study black hole fuelling and radiative feedback from AGN and star formation in the context of early-type galaxies (ETGs). In Section 5, we present the main results of the simulations. Finally, in Section 6, we summarize our conclusions.

## 2 PREVIOUS WORK

It has long been known that the bulk of the matter that enters black holes over the history of the Universe does so via radiatively efficient accretion (Soltan 1982; Yu & Tremaine 2002). The resulting pho-

tons are the clearest observational indication that SMBH accretion is taking place.

There is a prodigious amount of energy and momentum available during Eddington-limited bursts consequent to accretion, certainly enough to have a profound effect on the structure and dynamics of the interstellar medium (ISM).

### 2.1 Mechanical feedback

Many AGN are observed to have broad absorption lines (BALs) indicating strong outflows. Several physical processes operating near the SMBH could plausibly launch these winds (e.g. Proga et al. 2000) and they go under the heading of mechanical feedback regardless of the details of their origin (Ostriker et al. 2010). They are thought to be somewhat collimated and are thus only observed in 1/4 to 1/2 of all bright AGN. Recently, quantitative estimates of the kinetic energy in these outflows have become available (Moe et al. 2009; Dunn et al. 2010) and indicate that they contain 0.1–1 per cent of the energy in the radiative component of the AGN output. Similar outflows with large opening angles are observed to be driven by star formation in ultraluminous IR galaxies (ULIRGs; Rupke, Veilleux & Sanders 2005; Rupke & Veilleux 2011), although the velocities are lower than those driven by AGN.

This mechanical energy can couple to the ISM much more efficiently than the AGN photons, making this an attractive mechanism for AGN feedback. However, there are significant observational uncertainties in these kinetic wind energy estimates; the studies have only been carried out for a few objects, and there is no global constraint analogous to the Soltan (1982) argument that allows an estimate of the global mean efficiency of energy conversion to kinetic winds in AGN. If the Moe et al. (2009) estimate of the kinetic luminosity is correct and we assume that all of the mechanical energy and momentum are effectively deposited into the ISM, then mechanical feedback will dominate over radiative feedback for column densities less than  $10^{21}$ – $10^{22}$   $\text{cm}^{-2}$ .

#### 2.1.1 Simulations of mechanical feedback

Many groups have carried out substantially similar studies of AGN feedback in the context of galaxy mergers where the black hole accretion rate is given by the smaller of the estimated Bondi rate and the Eddington rate, while the AGN feedback is assumed to be purely thermal energy injected in the vicinity of the black hole. This is the basic model developed by Di Matteo et al. (2005) and Springel et al. (2005) and applied extensively to compare with observations of the quasar luminosity function, galaxy colours and more (e.g. Hopkins et al. 2005, 2006, 2008a,b). The same basic model was also used by Johansson, Naab & Burkert (2009), and all authors found that AGN feedback has a dramatic effect on galaxies provided that 5 per cent of the bolometric AGN output is transformed into thermal energy within 100 pc of the black hole by mechanical winds operating on smaller scales.

However, observations of gas dynamics near AGN have indicated that the actual efficiencies are a factor of 5–50 smaller than the value usually used in many of these simulations (Moe et al. 2009; Dunn et al. 2010). Booth & Schaye (2009) and Choi et al. (2012) have carried out careful studies of the underlying numerical and physical assumptions that go into this feedback model, the latter paper finding that including the radial momentum of the AGN ejecta in the calculation dramatically increases the efficiency of mechanical feedback.

Dubois et al. (2010) developed a model of AGN involving anisotropic injection of kinetic energy on scales similar to the resolution of the simulation. They implemented this model in the adaptive-mesh-refinement code `RAMSES` (Teyssier 2002) and studied the implications of this feedback model on the properties of black holes and galaxy clusters in cosmological simulations at a resolution of approximately 1 kpc.

Gaspari, Brighenti & Temi (2012) performed simulations of the evolution of the ISM of an elliptical galaxy in the presence of AGN feedback similar to that of Dubois et al. (2010). In terms of the galaxy model and the treatment of stellar evolution and mass loss, the simulations are substantially similar to those presented here. The differences include the fact that the Gaspari et al. (2012) simulations are three-dimensional rather than two-dimensional, have much lower spatial resolution ( $\simeq 150$  pc rather than 0.25 pc) and include feedback *only* via anisotropic injection of kinetic energy, rather than the more comprehensive feedback model presented here. Gaspari et al. (2012) found that mechanical feedback efficiencies in the range of those observed by Moe et al. (2009) and Dunn et al. (2010) were sufficient to limit black hole growth, balance atomic cooling and lead to observationally reasonable gas density and temperature profiles, in substantial agreement with the conclusions of Novak, Ostriker & Ciotti (2011), Ciotti, Ostriker & Proga (2010) and other studies.

The observational studies of Moe et al. (2009) and Dunn et al. (2010) indicate that this form of mechanical feedback only uses a small fraction of the available energy. This motivates the study of other forms of radiative feedback.

## 2.2 Radiative momentum feedback

It is well known that the photons couple to the ISM weakly if only the small Thompson cross-section is considered (e.g. Ciotti & Ostriker 2001). Of the momentum available, only a fraction  $\tau_{\text{ES}}$  (the optical depth to electron scattering) couples to the ISM, while there is no additional energy transfer to the gas in the case of pure Thompson scattering of photons having  $E \ll 1$  MeV. Only a small fraction of AGN are known to be optically thick to Compton scattering, although studies of the X-ray background indicate that Compton-thick AGN may be common at high redshift (Daddi et al. 2007). X-rays couple more strongly than lower energy photons (Sazonov et al. 2005) due to both inverse-Compton effects and coupling with resonant metal lines. Nevertheless, the  $M_{\text{BH}}-\sigma$  relation (Ferrarese & Merritt 2000; Gebhardt et al. 2000) has been construed as evidence that black holes regulate their growth via momentum-driven winds (King 2003).

Radiation also couples to the ISM through scattering/absorption by dust grains as well as atomic resonance lines. The cross-section for dust absorption in the ultraviolet (UV) for solar metallicity gas with a dust/gas ratio typical of the Milky Way can be 3500 times the electron scattering cross-section (Draine 2003), while that for resonance lines can be the same or greater (Proga et al. 2000; Sazonov et al. 2005). This means that radiative feedback due to line or dust absorption can provide more energy and momentum than mechanical feedback for column densities as low as  $10^{18}-10^{19}$  cm $^{-2}$ .

The potential importance of radiative momentum feedback has been known for some time (Haehnelt 1995; Ciotti & Ostriker 2007, hereafter C07), but the particular importance of dust in the context of AGN and starbursts was pointed out by Murray et al. (2005) and Thompson et al. (2005). The importance of this mechanism remains controversial – Socrates, Davis & Ramirez-Ruiz (2008,

appendix B) have argued that momentum cancellation owing to the fact that massive stars are distributed throughout the galaxy leads to a substantially reduced effect for the case of starbursts. However, this argument does not apply to momentum feedback driven by AGN. Simulations by Debuhr et al. (2010, 2011, 2012) explore the effect by modelling pressure acting on dust at radii large compared to the black hole but small compared to the galaxy. Note that while the physical process mediating the interaction between the SMBH and the ISM is different from the mechanical model of Di Matteo et al. (2005), the photon momentum is converted to hydrodynamic motion on scales smaller than the resolution of the simulation ( $\sim 100$  pc).

### 2.2.1 Simulations of radiative feedback

Sazonov et al. (2005) investigated the important effects of X-ray heating and Ciotti & Ostriker and collaborators have incorporated all of the standard electromagnetic processes into their one-dimensional treatments of the cooling flow initiated AGN outbursts (C07; Ciotti, Ostriker & Proga 2009b; Ciotti et al. 2010; Ciotti & Ostriker 2012). These investigations represent a different viewpoint from the ‘conventional’ view that AGN are associated with mergers. Here, the AGN activity is attributed to the reprocessing of gas lost by the evolving stellar population of an isolated and ‘passively’ evolving ETG. In Section 2.5, we comment on recent observations that bear on this point. Recently, Hensley, Ciotti & Ostriker (in preparation) have added an improved treatment of dust creation and destruction as well as a calculation of the dust temperature to these one-dimensional models.

Feedback in the Debuhr et al. simulations is implemented via a force on the gas assuming that there is a fixed optical depth to IR photon scattering by dust at all times ( $\tau \simeq 10$ ). No self-consistent solution for the radiation field is sought. The radiative force is applied over one resolution element near the black hole, so, although the physical model posits a radiative origin for the computed forces, in implementation their algorithm bears some resemblance to mechanical feedback schemes in that it is purely local and the photons do not exert forces over macroscopic distances in the simulation.

Novak et al. (2011) used the same physical model described in Sazonov et al. (2005) and C07 (with the exception of the radiative forces on dust) to run two-dimensional simulations of SMBH fuelling and AGN feedback. The present work extends Novak et al. (2011) to include radiative forces on dust grains. We seek to carry out the radiative transfer calculation due to photon absorption and scattering by dust in a self-consistent fashion.

Hambrick et al. (2011) and Kim et al. (2011) carried out simulations of black hole fuelling and AGN feedback during galaxy mergers and found that the addition of X-ray heating by the AGN allowed the black hole to regulate its own growth by keeping its immediate vicinity hot without necessarily heating the majority of the gas in the galaxy. Hambrick et al. (2011) used cosmological smoothed particle hydrodynamics (SPH) simulations with a simple treatment of X-ray photons from the AGN. Kim et al. (2011) performed adaptive-mesh simulations of galaxy mergers reaching a resolution of 15 pc. The simulations tracked mechanical feedback in the form of a collimated outflow generated near the black hole as well as radiative feedback in the form of X-rays generated by the AGN. The X-rays transferred energy and momentum to the surrounding gas, via a three-dimensional Monte Carlo ray-tracing algorithm.

### 2.3 Angular momentum transport

Several efforts have focused on understanding angular momentum transport in the absence of feedback. This eases one of the severe computational constraints in the problem since it is feedback that generates high gas temperatures and large gas velocities, necessitating very short simulation time steps and therefore very large computational costs per simulation. Levine et al. (2008) used adaptive-mesh cosmological simulations to examine gas transport from cosmological scales to  $\simeq 1$  pc from the black hole. Hopkins & Quataert (2010) carried out nested zoom-in simulations of the central regions of a galaxy undergoing a major merger. Both groups concluded that the mutual gravitational torques exerted by clumps of gas were sufficient to transfer angular momentum away from the central regions and permit accretion, and that the scale-free nature of gravity allowed the process to proceed in a nested fashion through all scales to the presumed black hole accretion disc. It is very attractive to split the problem of black hole fuelling and AGN feedback into a fuelling part and a feedback part. However, one would expect gas clumpiness to be dramatically reduced if AGN are able to heat the ISM significantly, which would in turn shut down the angular momentum transfer process that these authors envision. If the gas clumps are shielded from the AGN photons by a central dusty torus, or if the clumps of gas are self-shielding, then the process may continue to operate in spite of AGN feedback.

### 2.4 Subparsec simulations

As high-resolution simulation efforts that resolve the Bondi radius become more common, technical details of the numerical solution become important. Barai, Proga & Nagamine (2011) have performed a detailed study of the numerical and physical aspects of simulating Bondi accretion using SPH in the presence of heating by a central black hole over scales of 0.1–200 pc. They conclude that typical formulations of the artificial viscosity term typically used in SPH can cause excessive heating near the inner boundary of the simulation.

Dorodnitsyn, Kallman & Bisnovatyi-Kogan (2012) have studied the radiation hydrodynamics of the inner few parsecs of galaxies in the presence of dust in the flux-limited diffusion approximation. They show that the dusty torus around AGN is plausibly supported by radiation pressure on dust in an outflowing wind. They are interested in smaller physical scales than presently concern us, and they are only interested in the limit of large optical depths to scattering by dust in the IR. However, there is a significant overlap in the basic physics between their work and the present paper.

Roth et al. (2012) used a Monte Carlo method of obtaining the solution to the radiative transfer equation in three dimensions within 10 pc of an accreting black hole. The computed radiative forces were not coupled to the hydrodynamics – the purpose was to study the dependence of radiative forces on variation of the optical depth among different lines of sight. They found that the tendency of photons to escape through optically clear lines of sight reduces the overall effect of photon trapping, but that the total momentum imparted can still be as much as  $5L/c$ .

### 2.5 Observations concerning mergers, star formation and AGN

The observational situation regarding the links between black hole growth, star formation and mergers has been somewhat confused, although it seems that a preponderance of evidence is now indicating

that, although mergers may trigger AGN, the majority of AGN are *not* triggered by mergers.

Pierce et al. (2007) used a combination of X-ray data, space-based optical data and ground-based optical data, all part of the All-wavelength Extended Groth strip International Survey (AEGIS) survey (Davis et al. 2007), to conclude that X-ray-selected AGN preferentially reside in ETGs and that although the X-ray-selected AGN were more often members of close pairs, the companion was usually undisturbed. This was interpreted as evidence against interactions triggering AGN.

Using Sloan Digital Sky Survey data, Cisternas et al. (2011) found a strong correlation between close galaxy pairs and galactic star formation, but *no* correlation between close pairs and AGN activity. Schawinski et al. (2010) conducted a similar study and found superficially similar correlations, but based on their results connecting galaxy colour to stellar population age (Schawinski et al. 2007) they argued that the lack of AGN with close companions was due to a delay between the final merger and the onset of AGN activity.

Ellison et al. (2011) have found that close pairs tend to have AGN activity, but that AGN do not have an elevated close companion rate. They argue that mergers do indeed cause AGN activity, but that the majority of AGN are caused by other, presumably secular, processes.

Diamond-Stanic & Rieke (2012) found that AGN activity is correlated with *nuclear* star formation (within  $\sim 100$  pc), but *not* with *global* star formation on kiloparsec scales.

Schawinski et al. (2011) and Kocevski et al. (2012) used space-based optical and X-ray data to conclude that X-ray-selected AGN are not morphologically different from a mass-matched sample of quiescent galaxies.

As part of the Cosmic Assembly Near-infrared Deep Extragalactic Legacy Survey (CANDELS) survey (Grogin et al. 2011), Rosario et al. (2011) concluded that there is little difference between X-ray-selected AGN and quiescent galaxies in terms of colours and stellar populations out to a redshift of 3. All of this argues against a scenario where a large fraction of AGN are triggered by mergers.

## 3 THE RADIATIVE TRANSFER EQUATION

In this section, we develop a method of treating the radiative forces on the ISM gas in a galaxy. Our goal is to arrive at an algorithm that gives the correct behaviour in the many asymptotic limits required by the physical problem at hand.

First, we discuss the astrophysical requirements that motivate some of the choices we have made in defining the method. In the present work, we are primarily concerned with radiative forces on dust grains, but the method works for any source of isotropic scattering or absorption opacity.

More precisely, we derive three related algorithms for solving the radiative transfer equation. All of them arise from developing a set of moment equations for the specific intensity. For each method, we derive a set of differential equations, the solution of which gives the mean intensity and net flux of the photon field.

The first method (Section 3.2) gives a boundary value problem where the physical content of the set of differential equations is quite transparent. However, closing the set of differential equations in this method requires us to rely rather heavily on our physical intuition about the solution.

The second method (Appendix A) also gives boundary value problem and is more aesthetically pleasing in a formal mathematical sense because the closure relation is derived along with the set of

differential equations – it does not require a physically motivated guess. The cost is an additional differential equation to solve and the fact that the physical content of the equations is somewhat more opaque compared to the first method.

The third method (Appendix B) is an attempt to capture the essential behaviour of the system while reformulating it as an initial value problem. The reason for this is that it is vastly simpler to efficiently and robustly obtain the numerical solution to an initial value problem.

Note that in this work we use the first of these three methods and present the other two for reference and for future work. All three of the algorithms are self-consistent in the sense that we first solve for the photon field and then learn from this solution whether the radiation field is nearly isotropic (like the interior of a star) or highly directed (like a point source), whether the energy is carried by UV, optical or IR photons. We do not assume a priori that the system is in any particular asymptotic limit of the radiative transfer equation.

We neglect angular force terms, and although we use spherical symmetry to derive the differential equations, we argue in Section 3.2.1 that the method can be used with good results even in the case where the system is not spherically symmetric.

### 3.1 Astrophysical preliminaries

Over their lifetimes, galaxies explore essentially all of the asymptotic limits of the radiative transfer equation. Most of the time, most lines of sight are optically thin to radiation and the central SMBH is not accreting significantly, so the radiation field within the galaxy is nearly isotropic and produced by a spatially distributed source (the stars themselves). However, most galaxies undergo brief periods of intense SMBH accretion, during which time the radiation field is dominated by the central point source and is *not* isotropic. During these times, most lines of sight remain optically thin, but a few lines of sight pass through the central dusty torus which is highly optically thick to UV/optical photons. Furthermore, many galaxies probably have spent time in an LIRG/ULIRG state involving intense bursts of star formation with a nearly spherical, highly optically thick ISM in the central regions. In this case, the radiation field may be sourced primarily by the central point source or the distributed stars, and in either case repeated scattering and absorption of UV and optical photons make the radiation field tend towards isotropy. Overall, the galaxy does not spend much time in this highly optically thick state, but interesting and important things happen during that time.

It is crucial to note here that all of the energy absorbed in the UV/optical bands must be re-emitted as long-wavelength photons because to neglect the re-emission is to ignore energy and momentum conservation. In particular, ULIRGs are optically thick even to electron scattering over essentially all lines of sight, so the diffusion of the reprocessed IR photons can have a significant impact on the state of the gas in the galaxy (Murray et al. 2005; Thompson et al. 2005).

In the optically thin case, the radiation field is highly directed in the region where the point source dominates. This region always exists at sufficiently small radii for a true point source. If and when the stellar light starts to dominate the radiation field, it becomes nearly isotropic for radii within the region that is producing the bulk of the photons. For significantly larger radii, the radiation field again becomes directed as the photons emerge from the galaxy on nearly radial paths heading towards infinity.

If the ISM is optically thick to scattering, the radiation field quickly becomes isotropic even if the photons come from a central point source. In the UV and optical part of the spectrum, the

opacities to scattering and absorption due to dust are of the same order of magnitude. Typically the scattering opacity is less than the absorption opacity (Draine 2003), in which case the primary effect of scattering is to make the radiation field tend towards isotropy, rather than trapping photons so that they diffuse out of the galaxy. Therefore, in adopting a closure relation we will assume that the radiation field becomes nearly isotropic (although still maintaining a net outward flux) when the optical depth to scattering *or* absorption is greater than unity. If we assume that absorbed radiation is re-emitted in a different band, as we do in this work, and if the scattering opacity is *much smaller* than the absorption opacity, then this is incorrect: a highly directed radiation field from a point source is *always* highly directed even after many (absorption) optical depths. However, for realistic dust properties the scattering and absorption opacities are of the same order of magnitude.

If a UV or optical photon is absorbed rather than scattered, then the energy is reprocessed into the IR, but it is lost to the UV. Thus, if absorption *were* to strongly dominate over scattering, then the angular character of the radiation field (directed versus nearly isotropic) would tend not to change due to the effects of absorption alone. However, for declining density distributions, the column density  $\int \rho \kappa dr$  is dominated by what is occurring at small radii, whereas the energy injected by stars,  $\int \epsilon 4\pi r^2 dr$  (where  $\epsilon$  is the emissivity for stellar photons), is dominated by what is happening at large radii unless the stellar distribution falls off as  $r^{-3}$  or faster. Therefore, if the ISM is optically thick (to absorption), then the central point source will be diminished quickly compared to the isotropic radiation produced by stars even if absorption were to strongly dominate over scattering, leading to an isotropic radiation field over the bulk of the volume of the galaxy.

Radiative transfer is difficult in general, in part because of the high dimensionality of the problem. The quantities of interest are functions of spatial position, photon propagation direction, frequency and time, giving seven dimensions in total. Furthermore, the solution is subject to non-local effects: photons tend to leave a system via optically thin ‘windows’ if they are available. A nearly spherical gas cloud with optical depth  $\tau$  along most lines of sight and a few clear lines of sight comprising solid angle  $\Omega$  will trap photons roughly as though it had effective optical depth  $\tau_{\text{eff}} = \min(\tau, \Omega/4\pi)$ . That is, in order to effectively trap photons within an optically thick cloud, it is necessary to have a covering fraction of the order of  $1/\tau$  or else the photons will leak out of optically thin ‘holes’.

### 3.2 Mathematical treatment

Using the physical insight provided by the discussion in Section 3.1, we now seek a mathematical formulation of the problem that is not overwhelmingly computationally intensive and is correct (or nearly so) in each of the identified limits (optically thin/thick, radiation field nearly isotropic/highly directed, dominated by distributed source/point source and gas distribution nearly spherical/highly non-spherical).

We must distinguish the variables specifying the photon propagation direction from spatial position; to this end, we stipulate that  $\hat{\theta}$  and  $\hat{\phi}$  refer to spatial position, while  $\theta$  and  $\phi$  refer to photon propagation direction. Without loss of generality, in the case of isotropic scattering, as we consider in our treatment, the frequency-integrated equation of radiative transfer is

$$\frac{dI(\mu, \phi)}{ds} = -\rho(\kappa_a + \kappa_s)I + \rho\kappa_s J + \epsilon, \quad (1)$$

where  $s$  is the distance along the arbitrary direction of the ray,  $\mu = \cos \theta$ ,  $\theta$  is the angle between the ray propagation direction and the radial vector,  $\phi$  is the azimuthal angle,  $I \equiv dE/dt d\Omega dA$  is the specific intensity,  $J \equiv \int I d\mu d\phi/4\pi$  is the mean intensity,  $\rho$  is the gas density,  $\kappa_a$  is the cross-section for absorption per unit mass,  $\kappa_s$  is the cross-section for scattering per unit mass and, finally,  $\epsilon$  is the emissivity per unit solid angle (Chandrasekhar 1960). All quantities are functions of spatial position and time, suppressed above for brevity.

If we further adopt spherical symmetry, i.e. all quantities are independent of spatial position  $\theta$  and  $\phi$ , then equation (1) becomes

$$\mu \frac{\partial I}{\partial r} + \frac{1 - \mu^2}{r} \frac{\partial I}{\partial \mu} = -\rho(\kappa_a + \kappa_s)I + \rho\kappa_s J + \epsilon. \quad (2)$$

Here we seek a solution to this equation by taking moments in  $\mu$  and integrating away the dependence of the photon field on propagation direction. The final ingredient is a physically reasonable closure relation to terminate the set of moment equations, to be discussed below.

Note that although we write the radiative transfer equation in spherical form, the numerical method we outline does *not* require spherical symmetry. The gas density, opacities and photon field may vary as a function of  $\theta$  and  $\phi$ . Further details including the method by which this is accomplished as well as advantages and disadvantages of our formulation are discussed in Section 3.2.1.

The considerations in Section 3.1 can be summarized by the ansatz that the specific intensity is composed of three terms: one isotropic, one mildly anisotropic and one highly directed:

$$I = A + B\mu + D\delta(\mu - 1), \quad (3)$$

where  $\delta$  is the Dirac delta function and the three coefficients (which are functions of time and radial coordinate) are adjusted as described below. Incorporating the last term (with  $D > 0$ ) permits us to allow for phases when the central point-like quasar dominates the radiation field and to correctly treat the photon field far outside of the galaxy where the specific intensity resembles that of a point source. Note that if we were to take  $D = 0$  in equation (3), then we would arrive at the Eddington approximation, which is commonly adopted in stellar interiors. Taking equation (3) as a generalization of the Eddington approximation allows us to interpolate smoothly between the limits of a central point source and an optically thick situation.

Taking moments in  $\mu$  of the specific intensity to remove the explicit dependence on the ray propagation direction gives

$$J \equiv \frac{1}{4\pi} \int_0^{2\pi} d\phi \int_{-1}^1 I(\mu, \phi) d\mu = A + \frac{D}{4}, \quad (4)$$

$$F \equiv \int_0^{2\pi} d\phi \int_{-1}^1 \mu I(\mu, \phi) d\mu = \frac{4\pi B}{3} + \pi D \quad (5)$$

and

$$P \equiv \frac{1}{c} \int_0^{2\pi} d\phi \int_{-1}^1 \mu^2 I(\mu, \phi) d\mu = \frac{4\pi A}{3c} + \frac{\pi D}{c}, \quad (6)$$

where  $J$  is the mean intensity,  $F$  is the energy flux and  $P$  is the radiation pressure. We have taken the delta functions appearing at the edge of the integration domain to be equal to one-half in the above equations.

We must find some physically plausible way to decide whether the radiation field is nearly isotropic (in which case the standard Eddington closure relation  $P = u/3$  applies, where  $P$  is the radiation pressure and  $u$  is the energy density) or highly directed (in which

case the flux is simply related to the zeroth and second moments of the specific intensity).

To find the appropriate equations, we take two moments of equation (2) in two different cases. First, when the radiation field is mildly anisotropic ( $D = 0$ ) with the closure relation  $P = 4\pi J/3c$ , yielding the differential equations for the photon field in the classic Eddington approximation:

$$\frac{dL}{dr} = 4\pi r^2 (\dot{E} - 4\pi\rho\kappa_a J), \quad (7)$$

$$\frac{dJ}{dr} = -\frac{3\rho(\kappa_a + \kappa_s)L}{16\pi^2 r^2}, \quad (8)$$

where  $L = 4\pi r^2 F$  and  $\dot{E}$  is the energy in photons per unit volume per unit time produced by stars. Secondly, when the radiation field is highly directed ( $A = B = 0, D > 0$ ) with the closure relation  $P = 4\pi J/c$ , appropriate for a point source. In this case, the equation for  $dL/dr$  is the same and the equation for mean intensity becomes

$$\frac{dJ}{dr} = -\frac{2J}{r} - \frac{\rho(\kappa_a + \kappa_s)L}{16\pi^2 r^2}. \quad (9)$$

The first term on the right-hand side gives the expected  $r^{-2}$  fall-off of the mean intensity if the radiation field is primarily directed (e.g. outside of the galaxy).

We combine equations (8) and (9) for  $dJ/dr$  by introducing the variable  $t$  that interpolates between the optically thin (radiation field like a point source) and optically thick (radiation field nearly isotropic) cases. This gives

$$\frac{dL}{dr} = 4\pi r^2 (\dot{E} - 4\pi\rho\kappa_a J), \quad (10)$$

$$\frac{dJ}{dr} = -\frac{2Jt}{r} - \frac{(3-2t)\rho(\kappa_a + \kappa_s)L}{16\pi^2 r^2}, \quad (11)$$

where  $t = 0$  when the radiation field is nearly isotropic and  $t = 1$  when it is highly directed. In practice, we take  $t$  as a function of position:

$$1 - t(r) \equiv \frac{1}{1 + e^{5(1-\tau_{\text{out}})} + e^{5(1-\tau_{\text{in}})}}, \quad (12)$$

where

$$\tau_{\text{in}}(r) = \int_0^r \rho(\kappa_a + \kappa_s) dr \quad (13)$$

and

$$\tau_{\text{out}}(r) = \int_r^\infty \rho(\kappa_a + \kappa_s) dr. \quad (14)$$

Evaluating  $t$  as  $r$  becomes very large or very small gives  $t = 1$  at the inner boundary (near the AGN) and at the outer boundary (far from the galaxy). If the ISM is optically thick, there will be some region in between where  $t$  is nearly 0. This choice expresses our expectation about where the radiation field should be primarily directed versus primarily isotropic. The factors of 5 in equation (12) are chosen to ensure that the value of  $t$  switches from the optically thin limit to the optically thick limit fairly quickly near optical depths of unity. It is clear that the factors must be greater than unity in order for the radiation field to remain substantially point-source-like when the ISM is optically thin. The chosen factor of 5 ensures that transition effectively occurs between optical depths of 0.8 and 1.2. Choosing a smaller factor means that larger optical depths will be necessary before the algorithm switches to the radiation diffusion limit. That is, the specific intensity switches from being dominated by  $D$  to being dominated by  $B$ . In the limit of large optical depths,

the algorithm obtains the correct solution, and in the intermediate regime, the force on the ISM will be incorrect by at most a factor of 4/3 (equation 5).

Finally, we specify the boundary conditions. As in the study of stellar interiors, our second-order differential equation for  $L(r)$  requires two boundary conditions, one at the centre and one at the outer surface. Near the centre of the simulation, the outgoing luminosity is only that provided by the central point source, the AGN. Far from the galaxy, the radiation field is expected to again look like a point source as scattering/absorption become negligible and all of the photons leave the galaxy. The two natural boundary conditions are then

$$L(r_{\min}) = L_{\text{BH}} \quad (15)$$

and

$$J(r_{\max}) = \frac{L(r_{\max})}{16\pi^2 r_{\max}^2}. \quad (16)$$

The force on the gas in a computational cell is

$$\Delta f = \frac{L(r) d\tau dA}{4\pi r^2 c}, \quad (17)$$

where  $d\tau$  is the optical depth (scattering plus absorption) of a given cell and  $dA$  is the area of the cell perpendicular to the radiation flux vector.

### 3.2.1 Comments on the spherical symmetry assumption

We are primarily interested in what happens to the ISM as a function of radius rather than angle. Angular effects are important and it is of crucial importance to break spherical symmetry so that hydrodynamic instabilities such as convection and the Rayleigh–Taylor instability can operate. However, we are concerned mainly with *whether* gas makes it to small radii (and accretes on to the black hole) or to large radius (and escapes the galaxy), not *where* on the sphere the gas enters the SMBH or leave the galaxy. Thus, we neglect all angular radiative forces and formulate the radiative transfer as occurring exclusively along rays from the centre of the galaxy.

Similar approximations have been used in numerical simulations of photon and neutrino transport in supernovae for some time (e.g. Brandt et al. 2011, and references therein). One approach is to spherically average the matter distribution, solve for the radiation field and then calculate forces on matter via equation (17). Another approach is to treat each ray as a separate problem, in which case all intensive quantities (gas density, emissivity of stellar photons, etc.) are treated as though they are obtained over the whole sphere.

We found that the first approach has dramatic failure modes where it wildly overestimates the outward radial forces on the gas in certain situations. As an example, consider an optically thick cloud covering a small solid angle in an otherwise optically thin medium. In reality, UV photons deposit momentum in a thin layer at the surface of the cloud, and the total momentum imparted to the cloud depends on the solid angle of the cloud. However, spherically averaging the matter distribution may result in the ISM becoming optically thin at the cloud radius, and the solution for the photon field will indicate that the UV flux is high throughout the cloud. In this case, essentially all of the dust grains in the cloud are able to absorb UV photons and the momentum imparted to the cloud will be wildly overestimated.

Instead, treating each ray as a completely independent problem has much better behaviour in the sense that when the algorithm makes an error in computing the force on a particular gas cell,

fractional error tends to be of the order of unity rather than orders of magnitude. In the previous example, this method gives the correct force exerted by UV photons. For the IR photons, the method assumes that they must traverse the cloud on their way out of the galaxy, while in reality they would leave the system via the optically thin ambient medium. Therefore, the method makes a fractional error of the order of the IR optical depth when computing the force.

One drawback of the latter approach is that if a particular ray (e.g. near the pole) has deficient star formation compared to the rest of the galaxy, then the forces exerted by the stellar photons will be anaemic compared to the true solution, where stars from near the mid-plane emit photons that help push on gas near the poles. Therefore, we average source terms over a sphere before finding the solution to the radiative transfer equations on each ray.

Note that this method allows the radiation field to differ in an unlimited way from one ray to the next. This is expected, for example, in the UV where the scattering opacity is less than the absorption opacity, and the interior of an individual ‘cloud’ along a line of sight can be shielded from the AGN UV luminosity. However, in the IR we consider the absorption opacity to be zero, and it no longer makes sense that the radiation field could differ substantially on adjacent rays. Therefore, we also spherically average the IR source terms (in particular IR generated by absorption of UV or optical) before solving for the luminosity as a function of radius in the IR.

In the case where all lines of sight are optically thin, IR emitted isotropically should affect all gas at larger radius, whether the target lies along the same line connecting the source to the AGN or not, so spherically averaging the IR source terms brings us closer to the actual solution. In the case where all lines of sight are optically thick, the radiation field is expected to become isotropic and spherically symmetric as photons diffuse from the centre. In this case, too, spherically averaging the IR source terms brings us closer to the actual solution. The most delicate situation occurs when some lines of sight are optically thick, while other lines of sight are optically thin. The IR is emitted isotropically, so the IR flux at large radius should be significant even if the optical depth along that specific line of sight is small. Furthermore, the IR flux generated along a line of sight with large optical depth will tend to escape though optically clear holes rather than be ‘forced’ to diffuse out along the same line of sight upon which it was generated. Therefore, in this last case as well, spherically averaging the IR source terms brings us closer to the actual behaviour of the system.

### 3.3 Numerical implementation

The numerical solution of the radiative transfer equation is complicated by the fact that one boundary condition is specified at  $r_{\min}$ , while the other is specified at  $r_{\max}$  (note equations 15 and 16). Thus, integration from either side requires a guess that must be refined. This is identical to the situation in treating the radiative transfer in stellar interiors. Conceptually, this is simply because we know the central luminosity, but we do not know the *intensity* of the radiation field near the centre. If the scattering opacity is large, photons will build up in the galaxy forming a nearly isotropic radiation field until the gradient of the photon density is sufficient to drive photon diffusion out of the galaxy at the rate required to carry the specified luminosity.

In fact, the numerical solution to the radiative transfer equation in stellar interiors is considerably simpler than in the present problem because, within stars, one can exploit the fact that the plasma is everywhere close to local thermodynamic equilibrium. The plasma is assumed to quickly thermalize any energy sources or sinks so that

the plasma is well described by a single temperature at any point. In galaxies, the photon field is not close to the thermodynamic equilibrium and we must track energy as it is transferred from X-rays to UV photons and eventually to IR photons. Treating stellar interiors in an analogous way would mean tracking each energy band of photons separately as the star’s luminosity was transported through the plasma, from the primary MeV photons produced by fusion reactions, to the UV photons that eventually emerge from the photosphere.

To find the solution of equations (10) and (11) subject to the correct boundary conditions (equations 15 and 16), the ‘shooting method’ with Newton–Raphson iteration (Press et al. 1992) works well up to optical depths of a few. Beyond that, the absorbing gas acts as a very effective ‘screen’ that hides conditions near the centre of the simulation from those at the outer edge. This makes it very difficult to find the correct solution matching both boundary conditions at once. We would like to simulate AGN feedback in galaxies with gas surface density up to Compton-thick, implying an optical depth to dust absorption in the UV of several thousand. The shooting method is too unstable to use in this case.

It is true that, given such a large optical depth, very little of the primary UV radiation escapes the galaxy; it comes out in the IR. However, it is incorrect to discard the primary UV radiation completely, or to immediately transfer it to the IR. While this would correctly give the emergent energy, the UV radiation can have a very large effect near the centre of the galaxy before it is transferred to the IR. For solar composition and dust/gas ratios, they can limit the accretion rate to  $3 \times 10^{-4} L_{\text{Edd}}$ .

At large optical depths, the more powerful ‘relaxation’ iterative method (Press et al. 1992) is required to adjust the solution over the entire domain of integration, while ensuring that the proper boundary conditions are met at both ends of the interval. Newton’s method is used to iterate over trial solutions to arrive at the solution to the differential equations, where the independent variables of the Newton iteration are taken to be the values of  $L$  and  $J$  at each spatial point. The method takes the coupling between variables at neighbouring points into account, allowing the entire solution to be updated without overcompensating (which the shooting method is prone to do). Given a good initial guess for the iteration, the relaxation method finds a reasonably accurate solution even for very large optical depths. The initial guess is conveniently provided by the solution that pertained during the previous simulation time step.

Two additional numerical schemes are defined in Appendices A and B. The method described in Appendix A allows one to avoid using the variable  $t$  and its somewhat ad hoc definition in equation (12) at a cost of one additional differential equation to solve and a somewhat more opaque relationship between the equations and their physical content. The algorithm described in Appendix B is an attempt to preserve the basic physics of the method while transforming the system of differential equations from a boundary value problem to an initial value problem. This allows one to use a substantially simpler numerical method to obtain the solution.

## 4 HYDRODYNAMICAL SIMULATIONS

For the full simulations, we will use the two-dimensional numerical code described in Novak et al. (2011). The code implements sources and sinks of mass, energy and momentum relevant for an ETG including stellar mass loss from planetary nebulae, Type Ia and Type II supernovae. A full description of the input physics can be found in Novak et al. (2011) and Ciotti & Ostriker (2012). We describe

the simple treatment of dust creation and destruction used in the present work. We refer readers to Hensley et al. (in preparation) for a more complete implementation of dust physics applied to one-dimensional models.

### 4.1 Time-scales

The light crossing time of the galaxy is by far the shortest time-scale in the system and therefore, if the ISM is optically thin, photons are considered to act instantaneously for the purpose of our simulation. When the ISM becomes optically thick, the radiative diffusion time is

$$t_{\text{diff}} \simeq \frac{R\tau}{c}, \quad (18)$$

where  $\tau$  is the optical depth. Typically, the temperature of the ISM is not far from the virial temperature of the galaxy, so that the dynamical time and the sound crossing time are nearly equal. The latter is

$$t_{\text{S}} \simeq \frac{R}{c_{\text{s}}}. \quad (19)$$

Thus, the radiative diffusion time will be shorter than the dynamical time and sound crossing time as long as  $\tau \leq c/c_{\text{s}} \simeq 1000$ . For our purpose, radiative diffusion takes place primarily in the IR, and the maximum optical depth in the IR is of the order of 10. Therefore, the radiation field is considered to reach equilibrium instantaneously, and radiative forces are considered to act instantaneously. That is to say that we solve all of the radiation transfer equations assuming a steady state.

### 4.2 Photon energy bands

We divide the radiative energy output of the AGN into broad-bands where the relevant physics is significantly different: IR (below 1 eV), optical (for our purposes, non-ionizing: 1–13 eV), UV including soft X-rays where the absorption cross-section is greater than the Thompson cross-section (13–2000 eV) and hard X-rays where the interactions are dominated by Compton scattering ( $\geq 2$  keV). The assumed division of the AGN output into the different bands is given in Table 1.

The radiative transport in the X-ray band is relatively simple. Few AGN are observed to be Compton thick and our simulations rarely reach such a high column density, so the ISM is always treated as optically thin. X-rays dominate the heating of the gas to temperatures of the order of the galactic virial temperature. We treat heating and cooling due to photoionization and Compton heating/cooling by atomic lines via the formulae given in Sazonov et al. (2005). X-rays also affect the gas momentum via Compton scattering and photoionization. Compton scattering by X-rays is handled along with the bolometric AGN luminosity owing to the wavelength independence of the Compton cross-section. Momentum transferred

**Table 1.** Assumed unabsorbed AGN energy output by band (Sazonov, Ostriker & Sunyaev 2004) and dust opacities for solar metallicity gas with Milky Way dust-to-gas ratio expressed in terms of the electron scattering opacity,  $\kappa_{\text{ES}} = 0.4 \text{ cm}^2 \text{ g}^{-1}$ .

Band	Energy	Fraction	Dust opacity
X-ray	$E > 2 \text{ keV}$	0.1	
UV	$13 \text{ eV} < E < 2 \text{ keV}$	0.35	$3430 \kappa_{\text{ES}}$
Optical	$1 < E < 13 \text{ eV}$	0.25	$857 \kappa_{\text{ES}}$
IR	$E < 1 \text{ eV}$	0.3	$5.71 \kappa_{\text{ES}}$

to the ISM by photoionization is taken to be

$$\frac{dp}{dt} = \frac{H}{c}, \quad (20)$$

where  $H$  is the photoionization heating rate. It should be noted that this is a lower limit to the total effect of photoionization on the momentum of the ISM. The Sazonov formulae give the photo heating rate due to X-rays, but neglect the heating at lower energies due, for example, to optical and UV photons.

An exact treatment of the effect of optical and UV photons necessitates tracking the temperature as well as the ionization state of the gas – this quickly becomes prohibitively complex. Instead, we note that X-rays are required to raise the gas temperature to the same order as the virial temperature for a massive galaxy, and therefore drive an outflow into the IGM. Lower energy photons may affect the detailed state of the gas in the galaxy, but they cannot affect whether or not the gas remains bound to the galaxy. Compton heating can be important if the Compton temperature of a given object is large. However, for typical objects Compton heating and cooling are subdominant. While optical and UV photons acting on atomic resonance lines are unable to raise the gas temperature to the galactic virial temperature, they nevertheless contribute to the force on the ISM. For the time being we neglect them.

Radiative transport in the IR is similarly simple. At long wavelengths, the dust absorption opacity is much greater than the scattering opacity (Draine 2003). However, the absorbed energy is re-radiated by the dust grains and thus the process is more similar to scattering than true absorption. In order to conserve energy, we simply treat the process as scattering. Since no energy is ever lost from the IR band and must leave the galaxy eventually, the IR luminosity as a function of radius is simply the integral of all source terms within the radius.

The UV and optical bands are considerably more complex. Each band satisfies a separate set of differential equations given by equations (10) and (11). The boundary conditions and method of solution are as described in Sections 3.2 and 3.3, applied to each band separately. Radiation absorbed in both bands contributes to the IR.

### 4.3 Opacities

At a minimum, photons emitted from the stars and AGN impart momentum to the ISM via Compton scattering. The Compton cross-section is wavelength independent and coherent up to energies of the order of 511 keV, making the effect easy to treat numerically. The force on a cell is given by equation (17), where  $L$  is the bolometric luminosity of stars and the AGN within the radius  $r$ . This is correct even when the ISM is Compton thick because the process involves only scattering and no absorption (up to energies approaching 511 keV).

The effect of absorption by dust is more complicated because the opacities depend strongly on wavelength, and hence it is necessary to track the luminosity as a function of photon energy and radius. The dust opacities for each band for solar metallicity gas with a Milky Way dust-to-gas ratio are given in Table 1.

Finally, outgoing photons can be absorbed by resonant atomic lines. In the case that the atom enters an excited state, the photon produced by the decay of the excited state is emitted isotropically. Thus, the photons impart momentum, but no net energy to the gas. These bound-bound transitions can have very large opacities, but only over a narrow range of frequencies, so we neglect this effect in the present work. In the case of photoionization, the energy in excess of the binding energy goes into heating the gas, imparting

both energy and momentum to the gas. For optical and UV photons, accurate calculation of the photoionization opacity requires detailed knowledge of the temperature and ionization state of ISM gas that the present simulations lack. Therefore, we leave the inclusion of photoionization opacity in the optical and UV bands for future work. For the high-energy photons that dominate the heating of the gas (see the discussion in the previous section and Sazonov et al. 2004), the photoionization force is included through equation (20), as discussed above.

### 4.4 Dust creation and destruction

Dust in ETGs is thought to be produced primarily in planetary nebulae and asymptotic giant branch outflows, and destroyed in hot gas by sputtering. Draine & Salpeter (1979) give a theoretical estimate of the dust destruction time as a function of grain size:

$$t_{\text{destroy}} \equiv \frac{a}{|\dot{a}|} = 10^5 \text{ yr } a_{0.1} n_1^{-1} (1 + T_6^{-3}), \quad (21)$$

where  $a_{0.1} = a/0.1 \mu\text{m}$ ,  $n_1 = \rho/m_p \text{ cm}^{-3}$  and  $T_6 = T/10^6 \text{ K}$ . Dust is also commonly observed to be produced via supernovae. Therefore, when gas is added to the computational grid by explicit stellar source terms, we also add dust in proportion.

Draine (2009) has recently argued that dust grain growth is predominantly by gas-phase growth in the ISM rather than in supernovae. If this is the case, we should add an explicit dust source term that causes the dust-to-gas ratio to relax to a specified value when the gas is cold and star forming, regardless of whether all of the gas in the cell is actually processed through supernovae.

In this scenario, dust grains are thought to be built up by accretion of single atoms from the gas phase, the inverse of the process that destroys grains at high temperature. The only difference is that grain growth requires that a dust grain collides with a metal atom rather than a more abundant hydrogen atom. Metal atoms are both less abundant and move more slowly in thermal equilibrium. Therefore, the time-scale for creation is easily obtained by scaling from the destruction time-scale:

$$t_{\text{create}} = 10^5 \text{ yr } A^{3/2} Z^{-1} a_{0.1} n_1^{-1} T_6^{1/2} (1 + 10 T_6), \quad (22)$$

where  $A$  is the atomic weight of the atoms in question (here taken to be  $A = 12$  for carbon),  $Z = \rho_{\text{metal}}/\rho$  is the metallicity of the gas and the  $(1 + 10 T_6)$  term is added to ensure that dust creation takes place only at temperatures below  $10^5 \text{ K}$  in the simulation.

The dust density in a given cell is represented by a passively advected tracer field with appropriate source terms for dust creation and destruction. The source and sink terms for dust in a given cell are

$$\dot{\rho}_{\text{dust}} = -\frac{\rho_{\text{dust}}}{t_{\text{destroy}}} + \frac{\rho Z - \rho_{\text{dust}}}{t_{\text{create}}}. \quad (23)$$

Dust grain growth terminates when all of the metals are in dust grains. In this paper, the treatment of dust is significantly improved with respect to the basic approach in the series of papers by Ciotti & Ostriker; however, in Hensley et al. (in preparation), the dust treatment is discussed in full generality, albeit in the context of one-dimensional simulations.

Including advection, the partial differential equation for the dust density is

$$\begin{aligned} \frac{\partial \rho_{\text{dust}}}{\partial t} + \frac{1}{r^2} \frac{\partial(r^2 v_r \rho_{\text{dust}})}{\partial r} + \frac{1}{r \sin \theta} \frac{\partial(\sin \theta v_\theta \rho_{\text{dust}})}{\partial \theta} \\ = -\frac{\rho_{\text{dust}}}{t_{\text{destroy}}} + \frac{\rho Z - \rho_{\text{dust}}}{t_{\text{create}}}. \end{aligned} \quad (24)$$

The radiative force on a cell due to absorption by dust is obtained from equation (17):

$$\Delta F = \frac{\rho_D}{\rho} \frac{L(r) d\tau dA}{4\pi r^2 c}, \quad (25)$$

where  $d\tau$  is the optical depth *if* there were no dust depletion, and the effect of dust depletion is taken into account by the density ratio.

One possible improvement to our treatment of dust creation and destruction would be to track the dust size distribution directly via moments. Our current implementation essentially assumes that all dust grains are maintained with a given fiducial size of  $0.1 \mu\text{m}$  and are then eroded via sputtering or grown via metal atom deposition.

#### 4.5 Stellar source terms

Since stars are sources of UV and optical light that contribute to the solution to the radiative transfer equation discussed here, we briefly review our implementation of star formation and generation of star light. Gas that forms stars also contributes to the energy balance via supernovae, our implementation of which is discussed in detail in C07.

Gas is removed from the galaxy by star formation at the instantaneous rate given by the standard formula based on the Kennicutt (1998) law:

$$\dot{\rho}_{\text{gas}} = -\frac{\eta_{\text{form}} \rho}{t_{\text{form}}}, \quad \eta_{\text{form}} = 0.1, \quad (26)$$

$$t_{\text{form}} = \max(t_{\text{cool}}, t_{\text{dyn}}), \quad (27)$$

$$t_{\text{cool}} = \frac{3k_B T}{2n\Lambda(T)}, \quad t_{\text{dyn}} = \min(t_{\text{jeans}}, t_{\text{rot}}), \quad (28)$$

$$t_{\text{jeans}} = \sqrt{\frac{3\pi}{32 G \rho}}, \quad t_{\text{rot}} = \frac{2\pi r}{v_c(r)}, \quad (29)$$

where  $n^2 \Lambda(T)$  is the volumetric cooling function and  $v_c(r)$  is the circular velocity at radius  $r$  in the galaxy (Ciotti & Ostriker 2012).

Mass that is transferred from gas to stars at radius  $r$  is first transferred to a ‘forming’ state by convolving the star formation rate with an exponential kernel with a time constant of 3 Myr, designed to account for the finite minimum star formation given by the Kelvin–Helmholtz time-scale as well as the minimum stellar lifetime given by the combination of the Eddington luminosity and the nuclear energy available to a massive star:

$$\dot{\rho}_{\text{forming}}(t) = -\frac{1}{t_{\text{KH}}} \int_0^t \dot{\rho}_{\text{gas}}(t') e^{-\frac{t-t'}{t_{\text{KH}}}} dt'. \quad (30)$$

These stars also contribute photons to the UV/optical luminosity of the galaxy via convolution with a similar exponential kernel:

$$\frac{dL_B}{dV}(t) = -\frac{1}{t_B} \int_0^t \epsilon_B c^2 \dot{\rho}_{\text{gas}}(t') e^{-\frac{t-t'}{t_B}} dt', \quad (31)$$

where  $B$  refers to band and takes the values UV or optical. Values for  $\epsilon_B$  and  $t_B$  for each band are given in Table 2.

#### 4.6 Radiative cooling and heating

Photons generated by collisional excitation of atomic lines or free–free radiation can only cool the ISM insofar as the photons can

**Table 2.** Parameters governing stellar luminosities (see text for definitions).

Band	Fraction
$\epsilon_{\text{UV}}$	$8.65 \times 10^{-5}$
$\epsilon_{\text{Opt}}$	$1.24 \times 10^{-3}$
$t_{\text{UV}}$	2.57 Myr
$t_{\text{Opt}}$	154 Myr

actually escape. If the galaxy becomes optically thick to IR radiation, then these photons can contribute significantly to the forces experienced by gas in the ISM as they diffuse out of the galaxy. Therefore, we add the cooling radiation to the distributed UV (optical) source terms if the local gas temperature is above (below)  $10^5$  K. The radiative formulae are discussed in Ciotti & Ostriker (2012).

#### 4.7 Broad-line wind

Our simulations also include a treatment of the broad-line wind generated near the SMBH. This is implemented as an inflow term on the edge of the computational grid (Novak et al. 2011; Ciotti & Ostriker 2012). Although the present paper focuses on radiative AGN feedback, we summarize our implementation of mechanical feedback because it has a large effect on the regulation of black hole growth. See Novak et al. (2011) and Ostriker et al. (2010) for further discussion of mechanical feedback.

The BAL originating near the SMBH provides energy, momentum and mass from a wind to the ISM according to the equations (Ostriker et al. 2010)

$$\dot{M}_{\text{BH}} = \frac{\dot{M}_{\text{infall}}}{1 + \eta}, \quad \eta = \frac{2\epsilon_W c^2}{v_W^2}, \quad (32)$$

$$\dot{E}_W = \epsilon_W \dot{M}_{\text{BH}} c^2, \quad \dot{P}_W = \frac{2\epsilon_W c^2 \dot{M}_{\text{BH}}}{v_W} \quad (33)$$

and

$$\dot{M}_W = \frac{2\epsilon_W c^2 \dot{M}_{\text{BH}}}{v_W^2}, \quad (34)$$

where  $v_W$  is the velocity of the BAL, taken here to be  $10\,000 \text{ km s}^{-1}$ .

Independently of the mechanical feedback model, the radiative luminosity of the AGN is given by

$$L = \epsilon_{\text{EM}} \dot{M}_{\text{BH}} c^2, \quad (35)$$

where the electromagnetic efficiency is given by the advection-dominated accretion flow inspired (Narayan & Yi 1994) formula:

$$\epsilon_{\text{EM}} = \frac{\epsilon_0 A \dot{m}}{1 + A \dot{m}}, \quad (36)$$

and  $A = 100$  and  $\epsilon_0 = 0.1$ . The dimensionless mass accretion rate is

$$\dot{m} = \frac{\dot{M}_{\text{BH}}}{\dot{M}_{\text{Edd}}} = \frac{\epsilon_0 \dot{M}_{\text{BH}} c^2}{L_{\text{Edd}}}, \quad (37)$$

where  $L_{\text{Edd}}$  is the Eddington luminosity.

Although our other work has considered models where  $\epsilon_W$  is a function of the accretion rate, in the present work we assume that  $\epsilon_W$  is a constant with values given in Table 3. In previous papers, these are called A models, and we maintain that nomenclature here. Our A0 model has the same value of  $\epsilon_W$  as that adopted by

**Table 3.** Values for the mechanical wind efficiency considered in this work.

Model	$\epsilon_w$
A0	$5 \times 10^{-3}$
A2	$10^{-4}$

Di Matteo et al. (2005), and our A2 model has a lower value, favoured by recent observations (Moe et al. 2009; Dunn et al. 2010).

#### 4.8 Galaxy model

The total gravitational potential of the model galaxy is assumed to be a singular isothermal sphere plus a point mass for the central BH. This is in good agreement with observations of the total mass profile of ETGs (Gavazzi et al. 2007, 2008). For simplicity, we maintain this model in to the smallest radii, although more complicated models may be more appropriate inside of a fraction of the half-light radius. The velocity dispersion parameter of the isothermal potential is  $260 \text{ km s}^{-1}$ . The gas is not self-gravitating. The stellar distribution is given by a Jaffe profile with a total mass of  $3 \times 10^{11} M_\odot$  and a projected half-mass radius of 6.9 kpc. The mass-to-light ratio is assumed to be spatially constant and is equal to 5.8 in solar units in the *B* band at the present time. The structural and dynamical properties of these galaxy models are discussed in detail in Ciotti, Morganti & de Zeeuw (2009a).

The assumed net specific angular momentum of the stars providing gas in the simulation is thus taken to be given by

$$\frac{1}{v_\phi(R)} = \frac{d}{\sigma R} + \frac{1}{f\sigma} + \frac{R}{\sigma(2r_{\min}^2 + GM_{\text{BH},i}r_{\min}\sigma^{-2})^{1/2}}, \quad (38)$$

where  $v_\phi$  is the velocity in the azimuthal direction,  $R$  is the distance to the  $z$ -axis,  $\sigma$  is the central one-dimensional line-of-sight velocity dispersion for the galaxy model,  $M_{\text{BH},i}$  refers to the black hole mass at the start of the simulations and  $d$ ,  $f$  and  $r_{\min}$  are parameters controlling the angular momentum profile at small, intermediate and large radii, respectively. This gives solid body rotation at radii less than  $d$  and constant specific angular momentum at large radii. The values used here are  $d = 10 \text{ pc}$ ,  $f = 1$  and  $r_{\min} = 1.25 \text{ pc}$ . This gives rotation velocities comparable to those of the most slowly rotating elliptical galaxies (Emsellem et al. 2004, 2007).

The computational grid goes from 2.5 pc to 250 kpc in 120 logarithmically spaced radial zones and 30 evenly spaced angular zones. The initial gas distribution is proportional to the stellar distribution and totals  $6.4 \times 10^8 M_\odot$ , corresponding to a gas fraction of 0.2 per cent.

We note that although the galaxy model is spherically symmetric and the physics as implemented is either spherically symmetric or at least symmetric under inversions of the  $z$ -axis, numerical noise is quickly amplified chaotically in the simulations so that the physical state does not remain up/down symmetric for very long.

## 5 RESULTS

All of the simulations presented here use the method described in Sections 3.2 through 3.3 to solve for the photon field, where the true boundary value problem is solved via the relaxation method.

Figs 1 and 2 show two snapshots from the ‘fiducial’ A2 simulation with mechanical AGN feedback efficiency of  $\epsilon_w = 10^{-4}$  and all of the physics thus far described enabled. The dust-to-gas

ratio is initialized to the Milky Way value throughout the galaxy. This simulation uses the ‘standard’ recipe for dust grain creation where dust is created in supernova and dust grains do not grow via collisions with gas-phase metal atoms in the ISM. However, all gas that enters the simulation grid does so with a Milky Way dust-to-gas ratio.

Fig. 1 shows that near the centre of the galaxy, dust is efficiently destroyed so that forces on gas due to absorption of photons by dust grains are not very effective at preventing gas from falling into the centre of the galaxy. At large radius, the temperatures are sufficient for sputtering to be effective, but the gas densities are low enough that the grain destruction time-scale is long.

In this picture, cold gas is generated by unstable cooling of the ISM. Cold gas loses pressure support and falls towards the centre of the galaxy on a free-fall time-scale. Cold gas is generated from hot gas, and the dust grains in the hot gas have been eroded by sputtering for at least a cooling time. Therefore, radiative forces on dust grains do not play a major role in the dynamics. Even if dust grains are replenished in the ISM without being processed through stars as suggested by Draine (2009), the grain growth time-scale is at best comparable to the infall time-scale. Given their initially depleted state, dust grains must have many growth time-scales available in order to replenish the dust.

If radiative forces on dust are to play a role in black hole accretion, then the gas feeding the black hole either must never have been hot, or must be cold for a long time before approaching the black hole. If the gas had been hot, it cannot return to the cold phase until a cooling time has passed, sufficient to significantly deplete the dust grains. Cold gas that is not rotationally supported falls to the centre of the galaxy too quickly to build up significant dust. However, dust lanes are observed in a significant fraction of elliptical galaxies (Hawarden et al. 1981; van Dokkum & Franx 1995). If the black hole is fed by gas processed through a rotationally supported galactic-scale disc, then dust grains would have a chance to build up, while the gas spends a long time orbiting the black hole.

In our simulations, dust is not negligible in determining black hole growth, but neither is it dominant. Extreme assumptions about the dust-to-gas ratio ranging from no dust at all to constant Milky Way ratios make at best a factor of 2 difference in the mass added to the black hole.

Figs 3 and 4 show the cumulative distribution of the ratio of the black hole accretion rate to the Eddington rate. The differences are not huge, but in the A2 case, dust opacity apparently does prevent the black hole from reaching the Eddington rate: the maximum is about 20 per cent of the Eddington rate. The fraction of the time when the SMBH would be identified as a quasar ( $L/L_{\text{Edd}} > 0.1$ ) is moderate.

Figs 5 and 6 show the effect of various physical processes on the momentum balance of the ISM. These figures immediately show which physical processes dominate and which are negligible. It is important to note that these figures show the time-averaged force per unit volume, so the dominant forces could change in the midst intense bursts of AGN accretion and star formation.

Most of the forces act on each grid cell separately, making it easy to tabulate how much momentum each separate process imparts to the ISM. Mechanical momentum is different: it is injected at the first grid cell and then the conservation equations of hydrodynamics transport that momentum outwards until it mixes with the ISM and the wind stops. However, the wind termination is not abrupt and there are significant radial motions in the ISM even in the absence of a mechanical wind from the AGN, so determining the exact radius at which the mechanical wind deposits momentum

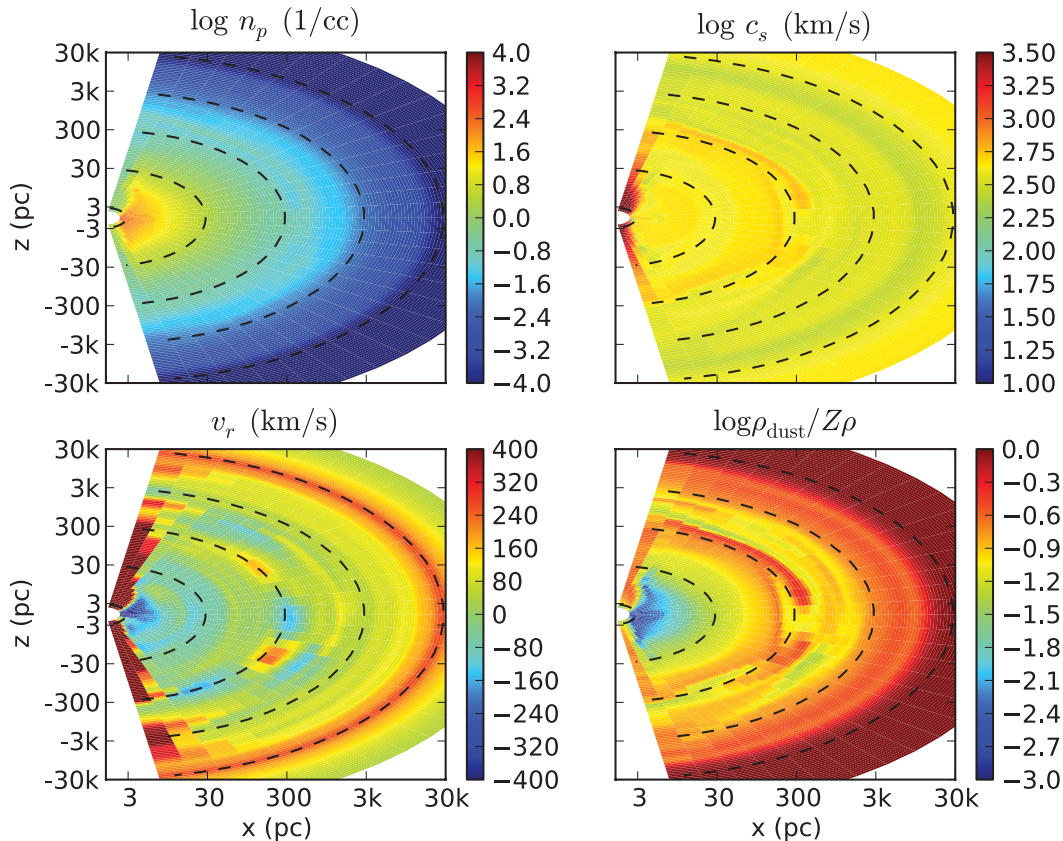


**Figure 1.** A snapshot of the A2 simulation during a quiescent phase. Upper left: log gas density in protons per cubic centimetre. Upper right: log sound speed. Lower left: radial velocity. Lower right: the log of the dust-to-gas ratio normalized to the value in the Milky Way. At small radii, densities and temperatures are large enough to efficiently destroy the dust grains, resulting in dust suppression by a factor of up to 1000. Gas that enters the ISM via the broad-line wind from the AGN is assumed to be dust rich. However, this gas is hot and rarefied, so the optical depth to dust absorption is roughly constant as a function of the polar angle, with a modest enhancement in the mid-plane.

is somewhat ambiguous. The quantity plotted as the red line in Figs 5 and 6 is the force per unit volume if the momentum is deposited uniformly within a sphere of radius  $r$ . Since the lines are also multiplied by  $(r/\text{kpc})^3$ , mechanical momentum shows up as a straight horizontal line. At very small radii, the ‘dentist drill’ effect ensures that not much radial momentum is actually mixed into the ISM. The mechanical wind typically does not extend to the outer edge of the simulation grid, so likewise little momentum is actually deposited at large radius. Therefore, the curve showing where the mechanical momentum is *actually* deposited would be low at small radii, low at large radii, nearly equal to the red line at intermediate radii (typically about 1 kpc) where the radial momentum from the wind is actually mixed into the ISM.

For the A2 simulation with dust destruction allowed, the most important sources of radial momentum are the mechanical wind, photoionization by AGN photons and absorption of UV AGN photons by dust grains. When dust destruction is not allowed and therefore the effects of dust are maximized, Fig. 6 shows that the most important sources of momentum are the mechanical wind, photoionization by AGN photons, and dust scattering and absorption of optical and IR photons originating from stars. In the latter, maximal dust case, the effect of stellar photons on dust grains becomes more important than the effect of AGN photons on dust grains for three reasons: (1) the black hole mass is about a factor of 2 smaller, so the black hole produces fewer photons; (2) about 20 per cent more stars

are formed, so stellar luminosity is increased; (3) the stars that form are *much* more centrally concentrated (about a factor of 2 more stars inside of 1 kpc), so the outgoing stellar photons see a larger optical depth to dust absorption because the density of the ISM falls steeply with radius.

Figs 5 and 6 both show that there is a strong rise in the amount of momentum imparted by UV photons produced by the AGN and absorbed by dust grains at the smallest radii covered by our simulations. This is expected for a configuration where the gas density falls more steeply with radius than  $r^{-1}$  and therefore the total optical depth depends strongly on the behaviour of the gas density and dust opacity at the innermost radii. However, we do not expect that the conclusions drawn from our present simulations would change if we adopted a smaller innermost radius because the presently adopted inner radius (2.5 pc) is of the same order as the expected value of the dust sublimation radius. Therefore, extending the simulations to smaller radii would necessitate the inclusion of dust destruction via sublimation, which would maintain the total optical depth to dust at values close to those obtained in the present simulations.

It is somewhat surprising that dust seems to have such a small effect on the black hole growth in the simulation, given that the opacity in the UV due to dust is 3500 times the electron scattering opacity. Therefore, at least in the ‘Max Dust’ case where a Milky Way dust-to-gas ratio is assumed for all gas, one might expect

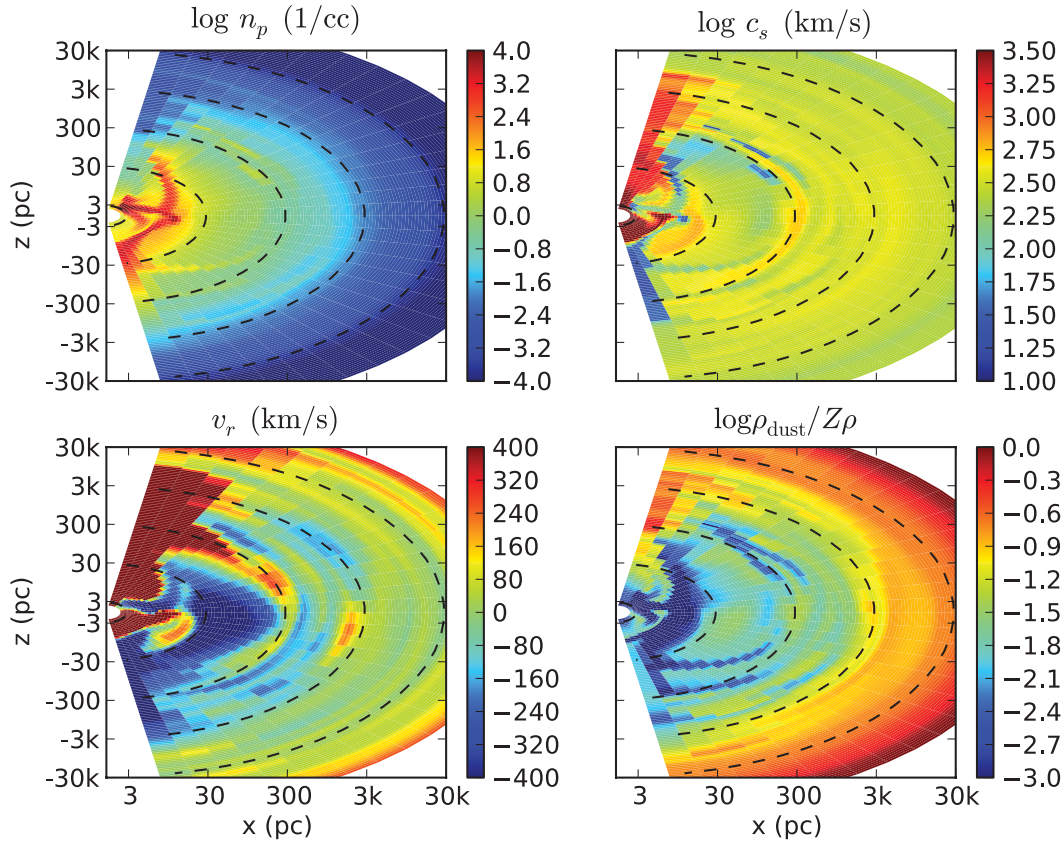


**Figure 2.** A snapshot of the A2 simulation during a black hole outburst. All gas near the centre of the galaxy is depleted of dust by a factor of at least 30 and up to 1000.

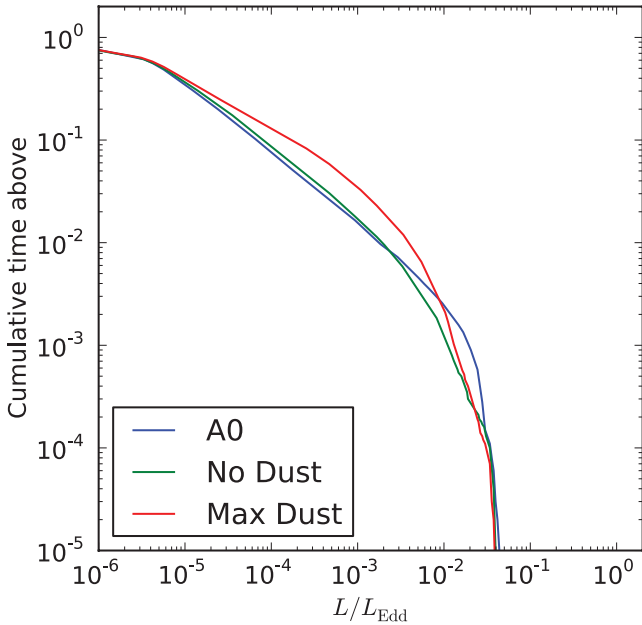


**Figure 3.** Cumulative time (in units of total elapsed time) where the ratio of the black hole accretion rate to the Eddington rate is above the given value for the A0 simulation with different assumptions about the dust-to-gas ratio. Dust does not make a big difference, although the ‘Max Dust’ simulation spends somewhat more time with an Eddington ratio of  $10^{-4}$  to  $10^{-2}$  compared to the other simulations.

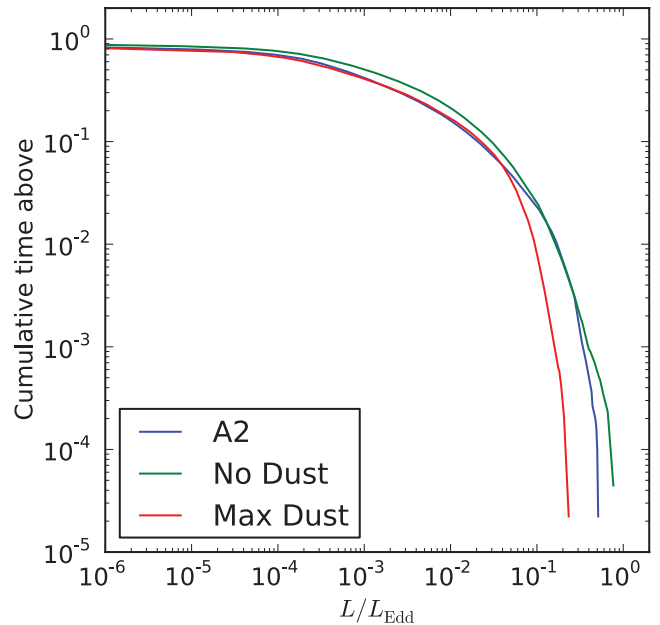


**Figure 4.** Cumulative time where the ratio of the black hole accretion rate to the Eddington rate is above the given value for the A2 simulation with different assumptions about the dust-to-gas ratio. Radiative forces on dust grains apparently prevent the black hole from reaching Eddington ratios greater than about 20 per cent.

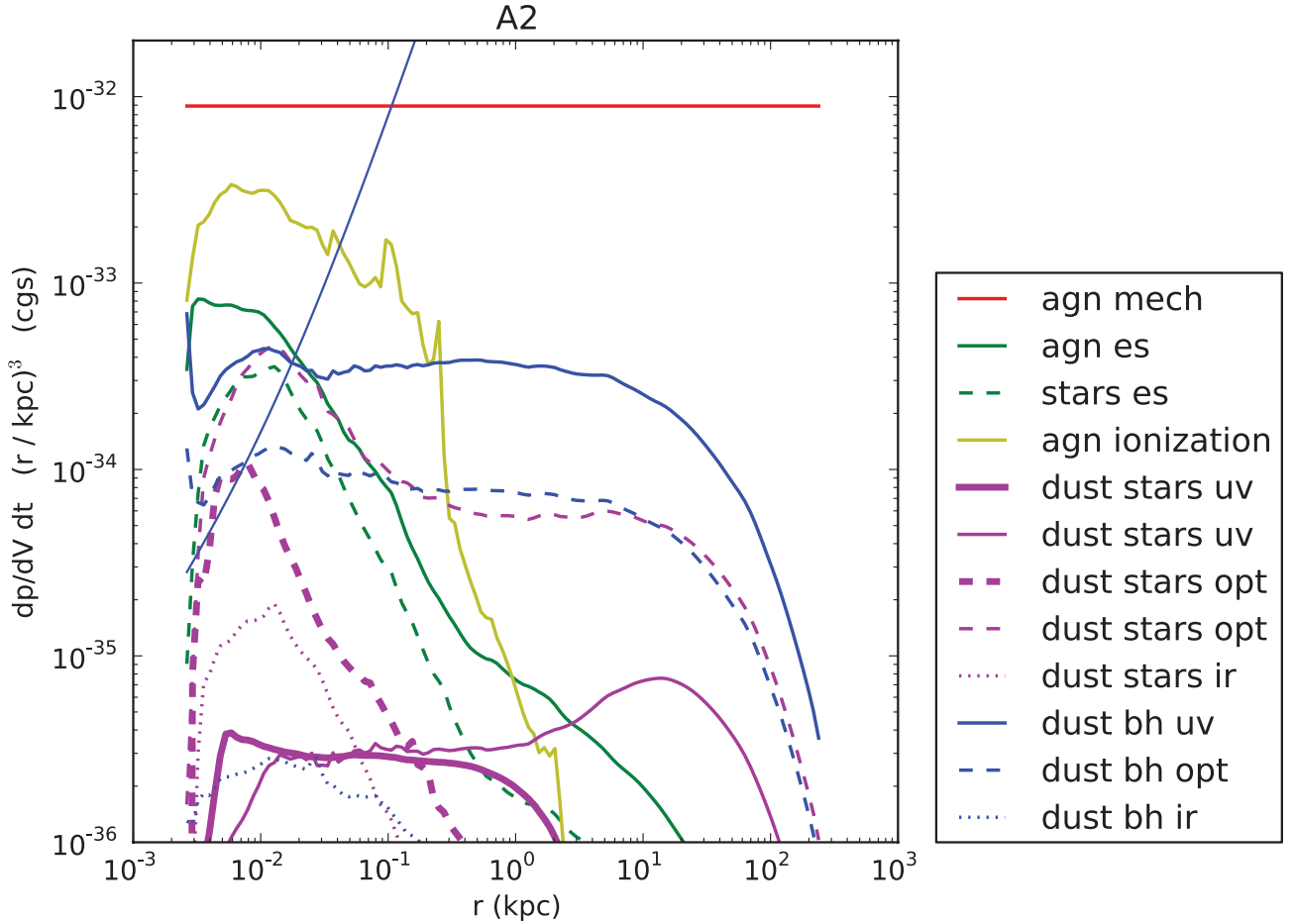


**Figure 5.** Time-averaged radial momentum source and sink terms over 1 Gyr for the A2 simulation. Each line shows the time-averaged force per unit volume imparted by each physical process as a function of radius. Curves have been multiplied by  $(r/\text{kpc})^3$  to flatten them out. The thin rising blue line is gravity. Heavy lines are forces directed inwards. Where a given physical process has both a heavy and light line, the force is sometimes directed inwards and sometimes directed outwards. The red line is for mechanical momentum. Mechanical momentum is injected at the first grid cell, so the quantity plotted is the force per unit volume if the momentum is deposited uniformly within a sphere of radius  $r$ . The green lines are for electron scattering of photons produced by the AGN or by stars, the yellow line is for photoionization by the AGN, the pink lines are for dust opacity for photons produced by the stars in different bands and the blue lines are for dust opacity for photons produced by the AGN in different bands. The mechanical momentum accounts for the bulk of the momentum injected by feedback, and it will dominate at the radius at which the momentum is actually deposited into the ISM (typically  $\simeq 1$  kpc). Photoionization by the AGN (AGN lines) is important inside a few hundred parsecs, outside of which AGN UV photons acting on dust are important.

that the effective limit to the black hole accretion rate is  $\sim 1/3500$  times the Eddington rate. However, the crucial difference is that radiative transfer is governed by the *absorption* opacity in the UV, while electron scattering and the transfer of thermal IR photons is a *scattering* problem. Once the UV has been absorbed, the radiative transfer in the IR is, again, essentially a scattering problem with  $\kappa_{\text{IR}} = 5.71\kappa_{\text{ES}}$ ; however, dust-to-gas ratios in elliptical galaxies are depleted as compared to the Milky Way by more than the modest factor of 5 required for electron scattering to dominate over dust scattering.

As noted by Thompson et al. (2005) and Murray et al. (2005) in the context of this problem, the force exerted on a shell of gas by photons where scattering dominates is

$$f = \frac{L\tau}{c}, \quad (39)$$

where  $L$  and  $\tau$  are the luminosity of the source and optical depth of the shell, both defined in the given frequency band. The energy in photons cannot be destroyed, so if the shell is optically thick, then photons build up until the gradient of the photon number density is

sufficient for diffusion to carry the input luminosity. This is why the Eddington luminosity effectively limits the black hole accretion rate even for Compton-thick sources, with the caveat that some energy is transferred to thermal energy in the gas by inelastic scattering of photons with energies of the order of 1 MeV. The Eddington limit remains the relevant limit until the optical depth to electron scattering becomes so large that the photon diffusion time is larger than the gas inflow time, in which case the photons are advected into the black hole along with the gas in a radiatively inefficient accretion flow.

However, the situation is quite different when the total opacity is dominated by absorption. For UV photons emitted by the black hole, the force exerted on a shell of gas is

$$f = \frac{L \min(\tau, 1)}{c}. \quad (40)$$

The incident UV photons deliver their momentum to the shell, after which they are converted to thermal IR photons where the opacity is much smaller. The thermal IR photons then simply leave the galaxy without further scattering until the galaxy becomes optically thick

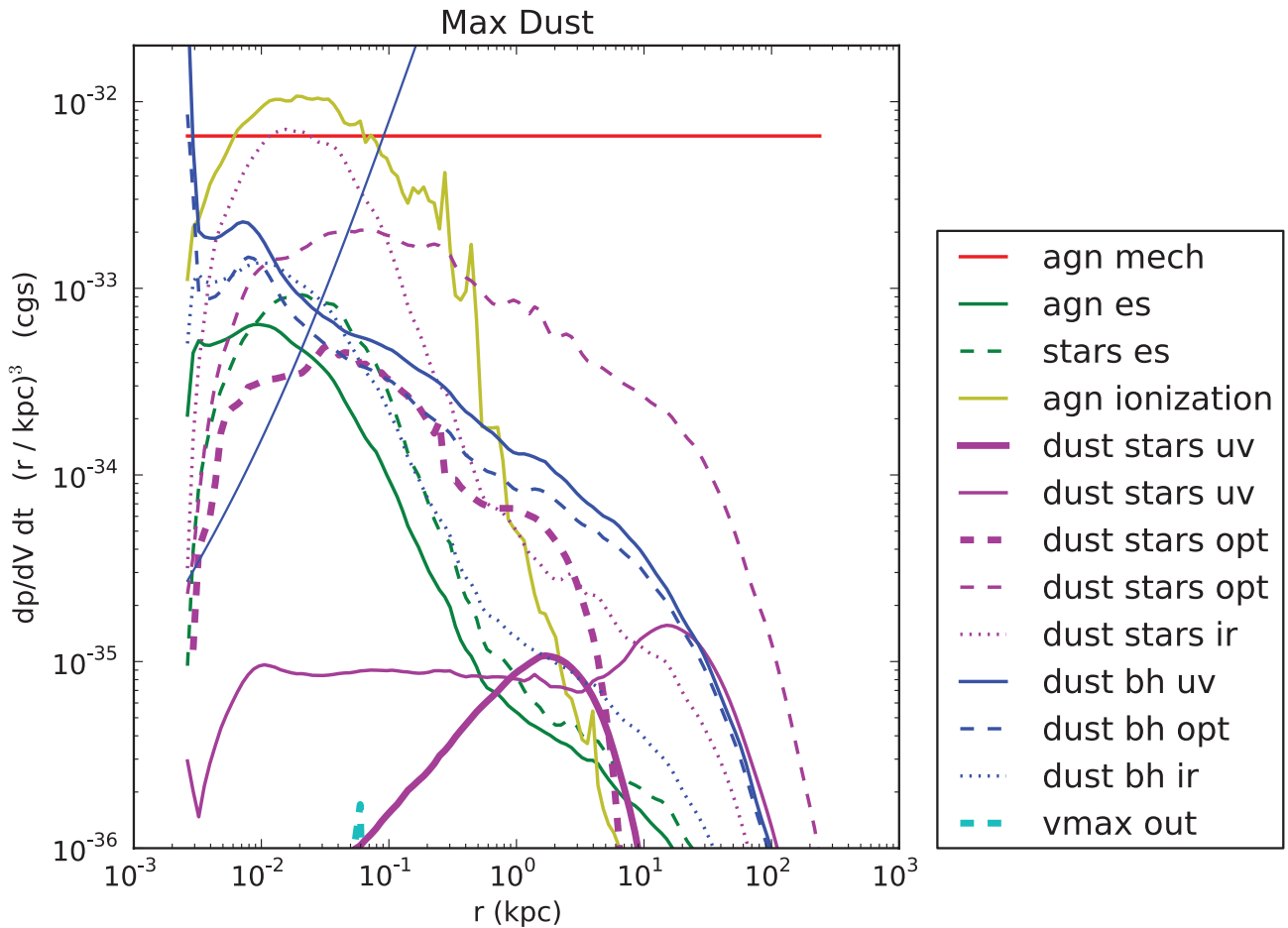


**Figure 6.** Radial momentum source and sink terms over 1 Gyr for the A2 simulation, assuming a Milky Way dust-to-gas ratio at all times. The lines and labels are the same as Fig. 5 except for the cyan line, which shows the very small amount of momentum removed by limiting the gas velocity to  $30\,000\text{ km s}^{-1}$ . The most important momentum sources are the mechanical wind, photoionization by the AGN and scattering of stellar IR photons by dust grains within about 1 kpc. Outside of 1 kpc, absorption of optical stellar photons by dust grains is the dominant source of momentum.

in the IR. The crucial point is that UV photons cannot build up and then diffuse out of the galaxy, as is the case when considering the electron scattering opacity and the dust opacity in the IR. The maximum force that can be exerted on a shell of gas is  $f_{\text{UV}}L/c$ , where  $f_{\text{UV}}$  is the fraction of the black hole bolometric luminosity that is emitted in the UV.

If the infalling clouds of gas are optically thin in the UV, then the force on a gas cloud is

$$f = \frac{L(f_{\text{UV}}\tau_{\text{UV}} + \tau_{\text{ES}})}{c} \simeq \frac{L\tau_{\text{ES}}}{c} \frac{f_{\text{UV}}\kappa_{\text{UV}}}{\kappa_{\text{ES}}}, \quad (41)$$

where  $L$  is the bolometric luminosity and  $f_{\text{UV}}$  is the fraction of the bolometric luminosity emerging in the UV. The cloud will feel a force much larger than if the dust opacity were not considered. However, if the cloud is optically thick in the UV (but not in the IR) then the force is

$$f = \frac{L(f_{\text{UV}} + \tau_{\text{ES}})}{c}. \quad (42)$$

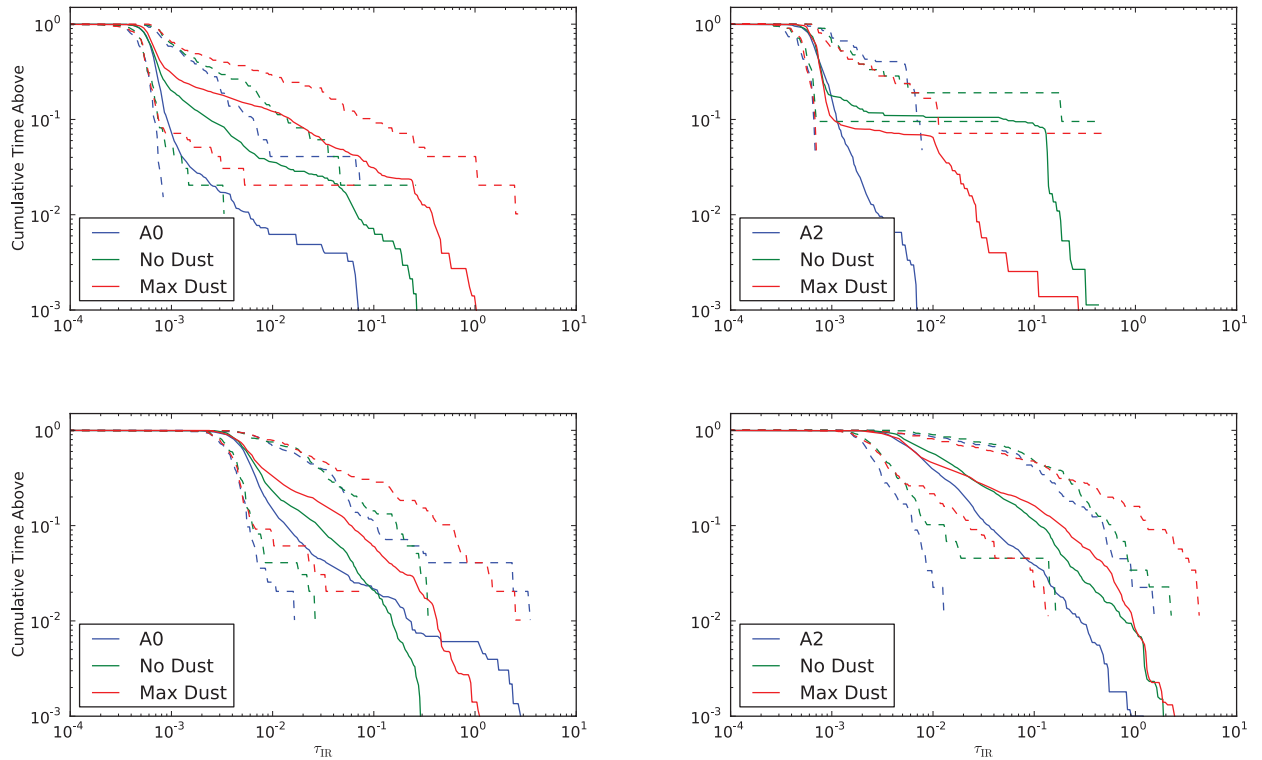
In this case, the force is nearly independent of the mass of the cloud; adding mass to an already optically thick cloud increases the gravitational force but not the opposing radiative force. This fact makes it difficult for the dust opacity in the UV to have a dramatic effect on the gas falling towards the black hole.

Fig. 7 shows the distribution of optical depths for the A0 and A2 simulations and variants. Note that all of the simulations include a

tracer field that tracks dust creation and destruction, whether that tracer field is involved in the calculation of radiative forces or not. This tracer field is used to compute the optical depths in the upper two panels of the figure. In the lower two panels, we have assumed a constant dust-to-gas ratio so that the optical depths scale strictly with the column density. Where the simulations differ is in how the radiative forces are computed: the ‘fiducial’ case uses the tracer field to compute dust opacities; the ‘Max Dust’ case uses only the column density along with an assumption about the global value of the dust-to-gas ratio; the ‘No Dust’ case ignores both the column density and the tracer field so that there are no radiative forces due to dust opacity.

The typical optical depths are far below unity, although a small fraction of the time the simulations become optically thick, at least along some lines of sight. However, the distribution of minimum optical depths for each simulation snapshot shows that there are almost always optically thin lines of sight available that will allow IR photons to escape without experiencing multiple scatterings that are necessary for equation (39) to be relevant.

In spite of dust having at best a minor effect on the dynamics of the ISM, it has a dramatic effect on the radiation emerging from the galaxy. With no dust grain destruction, the optical depth in the UV from the centre of the galaxy is typically of the order of unity. This means that the typical UV photon from the black hole is absorbed on its way out of the galaxy. Therefore, *observations*



**Figure 7.** In the upper two panels are shown the cumulative distribution of optical depths due to dust in the IR using the tracer field that tracks dust creation and destruction in the simulation to calculate the dust opacity. Note that all of the simulations include this tracer field whether it is used to compute radiative forces or not. The lower two panels show the same quantity assuming a constant dust-to-gas ratio (corresponding to values appropriate for the Milky Way) so that the optical depth scales directly with the column density of the gas. For solid lines, each line of sight in each snapshot contributes separately to the distribution. Dashed lines show the distributions where only the line of sight with the highest or lowest optical depth from each snapshot contributes. The simulations only rarely become optically thick in the IR, and when this happens, the optical depth is only a few times unity. Furthermore, the distribution of minimum optical depths shows that there are always optically thin lines of sight available that allow photons to exit the galaxy without scattering multiple times. For the simulations labelled ‘No Dust’, the simulation neglects any radiative forces associated with dust, but it nevertheless tracks the dust tracer field, allowing those simulations to be included in these plots.

of the AGN will be dramatically different for different assumptions about the creation and destruction of dust, even if the dust does not dramatically affect the dynamics of the galaxy.

Absorbed UV/optical photons from the AGN are converted to IR photons, but the galaxy is typically quite optically thin in the IR, so these photons escape without much fanfare. If the ISM were optically thick to IR photons, then they could have a dramatic effect as they scatter out of the galaxy, as pointed out by Murray et al. (2005) and Thompson et al. (2005), but we do not find the conditions necessary for this effect to prevail in our simulations. We find that in our detailed treatment of the radiative transfer, the factor  $\tau$  in equation (39) never exceeds unity by a significant amount.

Most stellar UV/optical photons are *not* absorbed because the star light is emitted at larger radius and need not traverse the densest part of the ISM. The typical stellar UV photon is produced at roughly the half-light radius of the galaxy, from which point the typical optical depth is far less than unity. Therefore, the stellar emission is largely unaffected by dust in the galaxy. The stellar photons that emerge from the galaxy are not greatly affected by dust, nor do the stellar photons strongly affect the dynamics of the ISM via dust opacity, even under dramatically different assumptions about the dust-to-gas ratio.

A subtlety arises when considering the distributed radiation source (the stars) in the case where the ISM is optically thick to absorption and the gas density is falling steeply (faster than  $r^{-1}$ ). In this case, it is possible for the luminosity at a given radius to be

negative, i.e. the net flux points inwards. If there were no absorption, then every ingoing photon would eventually become an outgoing photon, either by travelling unimpeded and emerging at a different point on the same sphere of radius  $r$ , or else by scattering until it diffused to radius  $r$ . This must be the case or else photons would build up at radii smaller than  $r$ .

However, when absorption is important, UV photons may propagate inwards, undergo absorption and re-emerge as IR photons. If the density profile is steep enough, this situation robustly leads to negative UV luminosities for radii smaller than the radius from which the typical UV photon is emitted. That is to say that the stars at larger radius exert a force acting to *compress* gas near the centre of the galaxy. The force is *not* balanced by outgoing IR photons (which must after all carry the energy of UV photons absorbed at small radius) because the opacity is smaller in the IR. The momentum carried by the IR photons is deposited at larger radius.

We find that this is often the case in our simulations: the gas density profile is generally steep enough to permit negative luminosities to develop within a few kiloparsecs of the centre of the galaxy. This effect can be seen in Figs 5 and 6.

There are situations in which dust plays a major role, such as galaxies undergoing starbursts or merger-induced quasar activity with copious quantities of cold gas (Murray et al. 2005; Thompson et al. 2005; Debuhr et al. 2010, 2011). We have performed one simulation designed to be similar to an ULIRG having a star formation rate of several hundred solar masses per year. The simulation

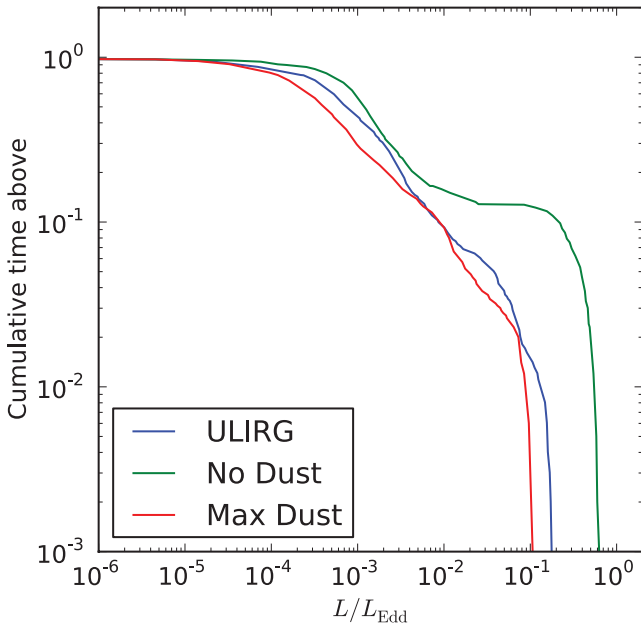


**Figure 8.** Cumulative time where the ratio of the black hole accretion rate to the Eddington rate is above the given value for a simulation designed to resemble a ULIRG with different assumptions about the dust-to-gas ratio. For large enough gas column densities, radiative effects due to dust opacity have a large effect, and a careful treatment of dust production and destruction produces results similar to the ‘Max Dust’ case, with ‘ULIRG’ SMBH luminosity in the quasar range for several per cent of the time.

uses the A2 feedback parameters but starts with  $3 \times 10^{10} M_{\odot}$  of gas, corresponding to a gas fraction of 10 per cent, as could be induced by a major merger or an inflow of cold gas. The star formation rate reaches peaks of 200 solar masses per year, approaching the ULIRG conditions.

Fig. 8 shows the distribution of Eddington ratios for different assumptions about the dust-to-gas ratio in this simulation. The simulation that includes dust creation and destruction is quite similar to the maximum dust case because the short dust creation time ensures that most of the gas has a dust-to-gas ratio near that of the Milky Way, as is observed in the ULIRG case. Assuming that there is *no* dust in the simulation yields a dramatically different distribution of Eddington ratios, reaching much larger values.

The time-averaged black hole accretion rates are  $0.045 M_{\odot} \text{ yr}^{-1}$  for the case with maximal dust,  $0.061 M_{\odot} \text{ yr}^{-1}$  for the case with dust creation and destruction, and  $0.32 M_{\odot} \text{ yr}^{-1}$  for the case with no dust. Thus, the presence of dust may suppress black hole growth by a factor of 5–7 depending on the assumptions surrounding dust creation and destruction.

These time-averaged accretion rates are to be compared to 0.0034, 0.0034 and  $0.0045 M_{\odot} \text{ yr}^{-1}$  for the A0 simulations with dust creation and destruction, no dust and maximal dust, respectively. In this case, dust has little effect on the dynamics of the simulation because the mechanical feedback dominates over everything else. For the A2 simulations, the time-averaged accretion rates are 0.092, 0.12 and  $0.072 M_{\odot} \text{ yr}^{-1}$  for simulations with dust creation and destruction, no dust and maximal dust, respectively. In this case, dust makes some difference, although it is not a dramatic effect. Furthermore, the detailed time evolution of the black hole mass shows that occasionally simulations with different assumptions about dust arrive at very similar black hole masses in spite of the black hole masses having been different at earlier times. This indicates that

sometimes the dust affects *when* gas reaches the black hole, but not *if* gas reaches the black hole.

It is important to remember that this system is highly non-linear and driven by stochastic events. If trivial changes are made to the initial conditions or to the implementation of the physics, then the black holes in the two simulations will grow in parallel with nearly the same mean accretion rate, but in a stochastic fashion. Depending on the state the system happens to be in at the moment when the simulation stops, one black hole mass could be larger than the other by several tens of per cent. This is the reason, for example, that the A0 Max Dust simulation has a larger mean accretion rate than the A0 No Dust simulation. Looking at several epochs as the simulation runs, one concludes that the black hole masses are tracking each other stochastically and therefore that dust does not play a crucial role in limiting the black hole’s growth in that case.

Fig. 9 is the analogue of Figs 5 and 6 for the ULIRG simulation, showing the effect of various physical processes on the momentum balance of the ISM. The dominant source of momentum from the AGN is the photoionization opacity, which dominates inside of 1 kpc. Scattering of stellar IR photons by dust grains is important inside of 1 kpc, and absorption of optical stellar photons by dust grains is important outside of 1 kpc. The momentum imparted by the broad-line wind is not negligible, but it does not dominate the momentum budget as it does in the other cases considered here.

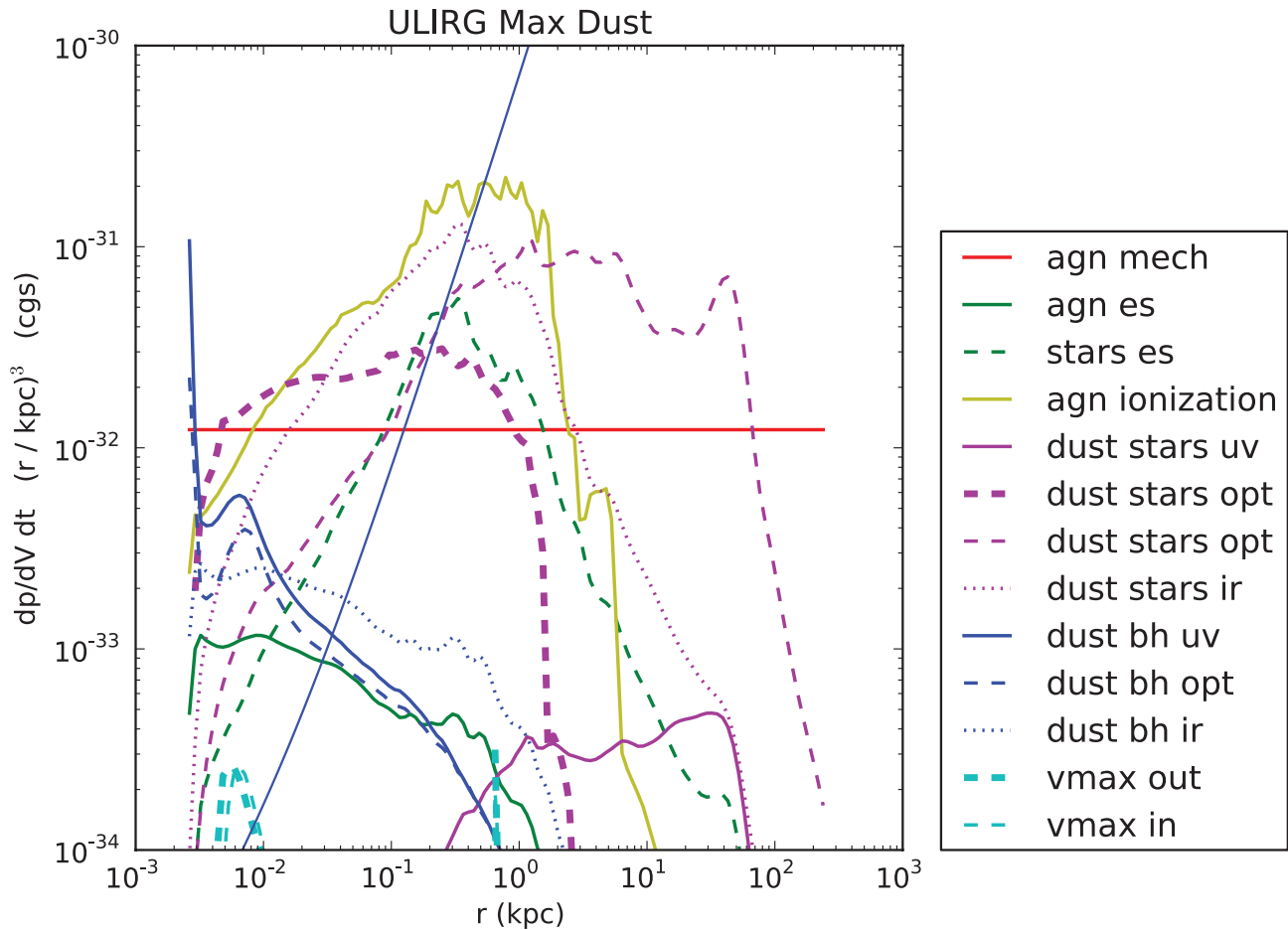
The reason that the presence of dust suppresses black hole growth in the ULIRG simulation but does not make a dramatic difference in the other cases is that the conditions in the ULIRG simulation resemble those envisioned by Thompson et al. (2005) and Murray et al. (2005): the gas surface density is high enough that the galaxy is optically thick in the IR. The IR photons build up in the galaxy until the gradient of the photon number density is sufficient to carry the black hole luminosity by photon diffusion. In this case, the relevant opacity to limit accretion is not the electron scattering opacity but the dust opacity in the IR. Dust then has a dramatic effect on the gas dynamics and on the growth of the black hole.

Fig. 10 shows the cumulative distribution of optical depths due to dust in the IR for the ULIRG-like simulation. We remind the reader that we spherically average the IR source terms before calculating forces on the ISM so that the IR flux at a given position includes IR generated at smaller radius on *all* lines of sight, as discussed in Section 3.2.1.

Along some lines of sight, the situation resembles that envisioned by Thompson et al. (2005) and Murray et al. (2005) for a significant but subdominant fraction of the time – optical depths are a few times unity and can exceed 10. However, the distribution of minimum optical depths for each simulation snapshot shows that IR photons would always be able to escape via optically thin ‘windows’. In order for equation (39) to pertain, the IR photons must be effectively trapped in the galaxy so that the only way for them to exit the galaxy is via diffusion. If there are optically thin lines of sight, this will not occur.

## 6 DISCUSSION AND CONCLUSIONS

We have outlined a method for computing the forces on interstellar gas due to absorption of photons by dust grains. The radiative transfer equation is recast into a set of differential equations by taking moments in the photon propagation direction. The set of differential equations comprises a boundary value problem, the solution of which gives the photon field which can be used to compute forces



**Figure 9.** Radial momentum source and sink terms over 1 Gyr for the ULIRG simulation, assuming a Milky Way dust-to-gas ratio at all times. The lines and labels are the same as Fig. 5. The most important momentum sources are photoionization by the AGN and scattering of stellar IR photons by dust grains within about 1 kpc. Outside of 1 kpc, absorption of optical stellar photons by dust grains is the dominant source of momentum. At very small radii, AGN photons absorbed by dust grains make a contribution. Note in particular that the heavy dashed magenta line that briefly dominates around 5 pc records the momentum imparted to the gas by *ingoing* stellar photons: it represents a force towards the black hole. See Section 5 for further discussion.

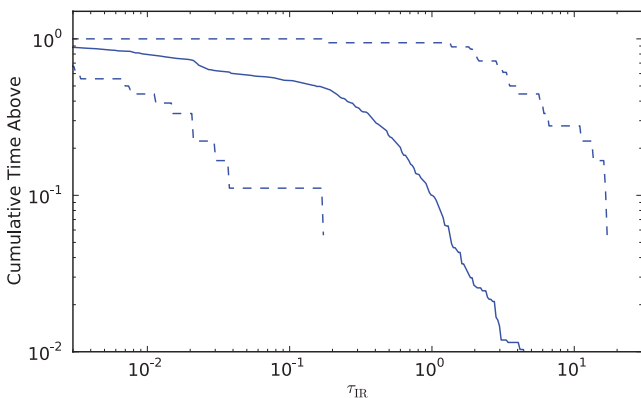


**Figure 10.** Cumulative distribution of optical depths due to dust in the IR for the simulation designed to resemble a ULIRG. The ‘Max Dust’ case is shown, but high gas densities resulted in sufficiently fast dust creation that the other cases do not differ significantly. Typical optical depths along a typical line of sight are of the order of unity. There are almost always optically thick lines of sight where the optical depth is larger than 10 for a significant fraction of the time. However, even in this case there are always optically thin lines of sight that would allow photons to easily escape from the galaxy.

on the ISM. We identified a numerical method that reliably gives the solution to the set of differential equations even for very large optical depths.

The method gives the correct asymptotic behaviour in all of the relevant limits (dominated by the central point source; dominated by the distributed isotropic source; optically thin; optically thick to UV/optical; optically thick to IR; photon field nearly isotropic; photon field highly directed) and reasonably interpolates between the limits when necessary. The method is explicitly energy conserving so that UV/optical photons that are absorbed are not lost, but are rather redistributed to the IR where they may scatter out of the galaxy. It does not require spherical symmetry, but it only handles the radial component of radiative forces.

We have also described a physically motivated simplification of the above method based on splitting the photon field into ingoing and outgoing streams. This method is much simpler to implement and shares many of the desirable characteristics of the more complicated method.

We have implemented both of these numerical methods in a hydrodynamic code with source terms for energy, momentum and mass appropriate to study black hole fuelling and star formation in ETGs. Both radiative and mechanical feedback are included for both the AGN and the stars. We allow for dust destruction by sputtering

and dust creation by supernovae, planetary winds and optionally gas-phase grain growth.

In the case of secular fuelling of a normal SMBH in an elliptical galaxy, the dynamics of the simulations are not greatly affected by the presence or absence of dust. At high AGN mechanical feedback efficiencies, dust has very little effect because mechanical feedback dominates. At lower mechanical feedback efficiencies, dust has some effect but large changes in our assumption about the dust-to-gas ratio lead to measurable but relatively modest changes in the black hole growth, star formation and galactic winds. This is true even for extreme assumptions about dust, ranging from no dust at all to assuming that dust-to-gas ratios pertaining to the Milky Way are appropriate at all times. Allowing for the possibility of dust destruction by sputtering in hot gas makes the simulations behave similarly to the ‘No Dust’ case.

Nevertheless, one mechanism by which dust opacity may contribute more substantially to the evolution of the galaxy would be via rotational support so that gas densities reached higher values than those achieved by our simulations, where we assume small specific angular momenta. This may justify the larger assumed IR optical depths in the Debuhr et al. (2010, 2011, 2012) simulations. We emphasize that the issue is not dust survival versus destruction since we have included cases with the maximum reasonable dust-to-gas ratio among our simulations.

If the galaxy is optically thick to IR photons, repeated scattering of these photons can have a dramatic effect on the momentum balance of the ISM. We have verified this by simulating a galaxy with a very large mass in the ISM, as might follow a major merger with a gas-rich galaxy, in which case the presence or absence of dust makes a large difference, as expected.

However, we do not find that this situation is typically realized in our simulations. The opacity of dust in the IR is about five times the electron scattering opacity, so a system must be Compton thick before this scattering starts to have a large effect. Our simulated galaxies are occasionally Compton thick, but no more, and they typically have much lower column densities. Even with no dust destruction, we find that the optical depth in the IR is at most a few times unity, and it reaches that value only for a small fraction of the total simulation time. We find that it is very rare for the optical depth in the IR to significantly exceed unity, as is assumed by Debuhr et al. (2010, 2011). When dust destruction is allowed, the optical depths in the IR are typically smaller by several orders of magnitude.

## ACKNOWLEDGMENTS

We thank Bruce Draine, Daniel Proga and Sergey Sazonov for useful discussions and the anonymous referee for a helpful report. GSN was supported by the Princeton University Council on Science and Technology, by the ERC European Research Council under the Advanced Grant Program No. 267399-Momentum, and made extensive use of the computing facilities of the Princeton Institute for Computational Science and Engineering. LC is supported by the MIUR grant CoFin08.

## REFERENCES

- Arav N., Dunn J. P., Korista K., Edmonds D., González-Serrano J. I., Benn C., Jiménez-Luján F., 2012, *ApJ*, submitted
- Barai P., Proga D., Nagamine K., 2011, *MNRAS*, 418, 591
- Binney J., Tabor G., 1995, *MNRAS*, 276, 663
- Booth C. M., Schaye J., 2009, *MNRAS*, 398, 53
- Brandt T. D., Burrows A., Ott C. D., Livne E., 2011, *ApJ*, 728, 8
- Chandrasekhar S., 1960, *Radiative Transfer*. Dover, New York
- Choi E., Ostriker J. P., Naab T., Johansson P. H., 2012, *ApJ*, 754, 125
- Ciotti L., Ostriker J. P., 1997, *ApJ*, 487, L105
- Ciotti L., Ostriker J. P., 2001, *ApJ*, 551, 131
- Ciotti L., Ostriker J. P., 2007, *ApJ*, 665, 1038 (C07)
- Ciotti L., Ostriker J. P., 2012, in Kim D.-W., Pellegrini S., eds, *Astrophys. Space Sci. Libr. Vol. 378, Hot Interstellar Matter in Elliptical Galaxies*. Springer, Heidelberg, p. 83
- Ciotti L., Morganti L., de Zeeuw P. T., 2009a, *MNRAS*, 393, 491
- Ciotti L., Ostriker J. P., Proga D., 2009b, *ApJ*, 699, 89
- Ciotti L., Ostriker J. P., Proga D., 2010, *ApJ*, 717, 708
- Cisternas M. et al., 2011, *ApJ*, 726, 57
- Croton D. J. et al., 2006, *MNRAS*, 365, 11
- Daddi E. et al., 2007, *ApJ*, 670, 173
- Davis M. et al., 2007, *ApJ*, 660, L1
- Debuhr J., Quataert E., Ma C., Hopkins P., 2010, *MNRAS*, 406, L55
- Debuhr J., Quataert E., Ma C.-P., 2011, *MNRAS*, 412, 1341
- Debuhr J., Quataert E., Ma C.-P., 2012, *MNRAS*, 420, 2221
- Di Matteo T., Springel V., Hernquist L., 2005, *Nat*, 433, 604
- Diamond-Stanic A. M., Rieke G. H., 2012, *ApJ*, 746, 168
- Dorodnitsyn A., Kallman T., Bisnovatyi-Kogan G. S., 2012, *ApJ*, 747, 8
- Draine B. T., 2003, *ARA&A*, 41, 241
- Draine B. T., 2009, in Henning T., Grün E., Steinacker J., eds, *ASP Conf. Ser. Vol. 414, Cosmic Dust – Near and Far*. Astron. Soc. Pac., San Francisco, p. 453
- Draine B. T., Salpeter E. E., 1979, *ApJ*, 231, 77
- Dubois Y., Devriendt J., Slyz A., Teyssier R., 2010, *MNRAS*, 409, 985
- Dunn J. P. et al., 2010, *ApJ*, 709, 611
- Ellison S. L., Patton D. R., Mendel J. T., Scudder J. M., 2011, *MNRAS*, 418, 2043
- Emsellem E. et al., 2004, *MNRAS*, 352, 721
- Emsellem E. et al., 2007, *MNRAS*, 379, 401
- Ferrarese L., Merritt D., 2000, *ApJ*, 539, L9
- Gaspari M., Brighenti F., Temi P., 2012, *MNRAS*, 424, 190
- Gavazzi R., Treu T., Rhodes J. D., Koopmans L. V. E., Bolton A. S., Burles S., Massey R. J., Moustakas L. A., 2007, *ApJ*, 667, 176
- Gavazzi R., Treu T., Koopmans L. V. E., Bolton A. S., Moustakas L. A., Burles S., Marshall P. J., 2008, *ApJ*, 677, 1046
- Gebhardt K. et al., 2000, *ApJ*, 539, L13
- Grogin N. A. et al., 2011, *ApJS*, 197, 35
- Gültekin K. et al., 2009, *ApJ*, 698, 198
- Haehnelt M. G., 1995, *MNRAS*, 273, 249
- Hambrick D. C., Ostriker J. P., Naab T., Johansson P. H., 2011, *ApJ*, 738, 16
- Hawarden T. G., Longmore A. J., Tritton S. B., Elson R. A. W., Corwin H. G., Jr, 1981, *MNRAS*, 196, 747
- Hopkins P. F., Quataert E., 2010, *MNRAS*, 407, 1529
- Hopkins P. F., Hernquist L., Cox T. J., Di Matteo T., Martini P., Robertson B., Springel V., 2005, *ApJ*, 630, 705
- Hopkins P. F., Hernquist L., Cox T. J., Di Matteo T., Robertson B., Springel V., 2006, *ApJS*, 163, 1
- Hopkins P. F., Hernquist L., Cox T. J., Kereš D., 2008a, *ApJS*, 175, 356
- Hopkins P. F., Cox T. J., Kereš D., Hernquist L., 2008b, *ApJS*, 175, 390
- Johansson P. H., Naab T., Burkert A., 2009, *ApJ*, 690, 802
- Kennicutt R. C., 1998, *ApJ*, 498, 541
- Kim J.-h., Wise J. H., Alvarez M. A., Abel T., 2011, *ApJ*, 738, 54
- King A., 2003, *ApJ*, 596, L27
- Kocevski D. D. et al., 2012, *ApJ*, 744, 148
- Kollmeier J. A. et al., 2006, *ApJ*, 648, 128
- Kurosawa R., Proga D., 2009, *ApJ*, 693, 1929
- Levine R., Gnedin N. Y., Hamilton A. J. S., Kravtsov A. V., 2008, *ApJ*, 678, 154
- Moe M., Arav N., Bautista M. A., Korista K. T., 2009, *ApJ*, 706, 525
- Murray N., Quataert E., Thompson T. A., 2005, *ApJ*, 618, 569
- Narayan R., Yi I., 1994, *ApJ*, 428, L13
- Novak G. S., Faber S. M., Dekel A., 2006, *ApJ*, 637, 96
- Novak G. S., Ostriker J. P., Ciotti L., 2011, *ApJ*, 737, 26
- Ostriker J. P., Choi E., Ciotti L., Novak G. S., Proga D., 2010, *ApJ*, 722, 642
- Park K., Ricotti M., 2011, *ApJ*, 739, 2

- Park K., Ricotti M., 2012, ApJ, 747, 9  
 Pierce C. M. et al., 2007, ApJ, 660, L19  
 Press W. H., Teukolsky S. A., Vetterling W. T., Flannery B. P., 1992, Numerical Recipes in C: The Art of Scientific Computing, 2nd edn. Cambridge Univ. Press, Cambridge  
 Proga D., Stone J. M., Kallman T. R., 2000, ApJ, 543, 686  
 Proga D., Ostriker J. P., Kurosawa R., 2008, ApJ, 676, 101  
 Rosario D. J. et al., 2011, preprint (arXiv:1110.3816)  
 Roth N., Kasen D., Hopkins P. F., Quataert E., 2012, preprint (arXiv:1204.0063)  
 Rupke D. S. N., Veilleux S., 2011, ApJ, 729, L27  
 Rupke D. S., Veilleux S., Sanders D. B., 2005, ApJS, 160, 115  
 Sazonov S. Y., Ostriker J. P., Sunyaev R. A., 2004, MNRAS, 347, 144  
 Sazonov S. Y., Ostriker J. P., Ciotti L., Sunyaev R. A., 2005, MNRAS, 358, 168  
 Schawinski K., Thomas D., Sarzi M., Maraston C., Kaviraj S., Joo S., Yi S. K., Silk J., 2007, MNRAS, 382, 1415  
 Schawinski K., Dowlin N., Thomas D., Urry C. M., Edmondson E., 2010, ApJ, 714, L108  
 Schawinski K., Treister E., Urry C. M., Cardamone C. N., Simmons B., Yi S. K., 2011, ApJ, 727, L31  
 Socrates A., Davis S. W., Ramirez-Ruiz E., 2008, ApJ, 687, 202  
 Soltan A., 1982, MNRAS, 200, 115  
 Springel V., Di Matteo T., Hernquist L., 2005, ApJ, 620, L79  
 Teyssier R., 2002, A&A, 385, 337  
 Thompson T. A., Quataert E., Murray N., 2005, ApJ, 630, 167  
 Tremaine S. et al., 2002, ApJ, 574, 740  
 van Dokkum P. G., Franx M., 1995, AJ, 110, 2027  
 Woo J., Urry C. M., 2002, ApJ, 579, 530  
 Yu Q., Tremaine S., 2002, MNRAS, 335, 965

## APPENDIX A: THIRD-ORDER RADIATION TRANSPORT

The quality of a solution to the radiation transport equation obtained by taking moments depends on the accuracy of the physical assumptions implicit in the chosen analytic form for the specific intensity. If those assumptions are not satisfied, taking the expansion to higher order is unlikely to provide benefits commensurate with the costs in terms of complexity and computational resources. We believe that the assumptions embodied by equations (3) and (12) are quite reasonable for the problem at hand. Nevertheless, it is possible to avoid using equation (12) by taking one additional moment of the specific intensity and radiation transport equation. We provide the equations here for reference but do not pursue the method further in the present paper.

Define the third moment of the specific intensity to be

$$Q \equiv \int_0^{2\pi} d\phi \int_{-1}^1 \mu^3 I(\mu, \phi) d\mu. \quad (\text{A1})$$

Given equation (3), we find

$$Q = \frac{4\pi B}{5} + \pi D. \quad (\text{A2})$$

We have three constants in the assumed form of the mean intensity and four moments of the mean intensity, so we can solve for the closure relation:

$$Q = \frac{3F + 3cP - 4\pi J}{5}. \quad (\text{A3})$$

To obtain the differential equations, we take the equations for the zeroth and first moment derived above, supplement them with the second moment of the radiation transport equation and then insert

the closure relation to obtain the following set of three equations:

$$\frac{dJ}{dr} + \frac{J}{r} + \frac{F}{\pi r} - \frac{3cP}{4\pi r} = -\rho \left( 3\kappa_a + \frac{5\kappa_s}{3} \right) J + \frac{\dot{E}}{3\pi} + \frac{\rho(\kappa_a + \kappa_s)(5cP - 3F)}{4\pi}, \quad (\text{A4})$$

$$\frac{dL}{dr} = 4\pi r^2 (\dot{E} - 4\pi \rho \kappa_a J) \quad (\text{A5})$$

and

$$c \frac{dP}{dr} - \frac{4\pi J}{r} + \frac{3cP}{r} = -\rho(\kappa_a + \kappa_s) F. \quad (\text{A6})$$

Adopting the use of these equations and closure relation is perhaps formally more appealing than the method outlined in Section 3. However, the cost is one additional equation to integrate and perhaps less obvious physical content to the closure relation and the equations themselves. We have included the present equations for reference, but do not use this method of obtaining solutions to the radiation transport problem in the present work.

## APPENDIX B: SIMPLIFIED RADIATION TRANSPORT

In Section 3, we have described a complete algorithm to solve for the photon field and, subsequently, the radiative forces on interstellar gas. The algorithm is exact in the sense that if the physical approximations used in its derivation are correct, the method will compute the correct photon field and radiative forces.

However, solving for the radiation field dominates the computational resources required for the calculation primarily because the system differential describes a boundary value problem rather than an initial value problem and hence finding the solution requires iteration. We would like *another* solution method that is *computationally* efficient while respecting the essential physics of the previously defined algorithm.

Consider the problem where the only source of radiation is the black hole and the scattering opacity is zero. The UV/optical photons are always radially outgoing at all times. Some UV/optical photons are converted to IR photons which diffuse out of the galaxy, but the UV/optical radiation field never becomes isotropic. In this case, the flux is simply related to the mean intensity ( $F = 4\pi J$ ) and we can eliminate equation (11) to obtain the single equation for the UV and optical components:

$$\frac{dL}{dr} = -\rho \kappa_a L. \quad (\text{B1})$$

The boundary condition is  $L(r_{\min}) = L_{\text{BH}}$ . This is now an initial value problem rather than a boundary value problem, and can be trivially solved by integrating from the inner edge of the simulation grid.

This change greatly simplifies the solution procedure. It would be very useful to obtain a simple approximate treatment of this problem as an initial value problem rather than a boundary value problem. We seek such an algorithm presently.

### B1 Differential equations

Conceptually, there are two streams of radiation: an ingoing stream and an outgoing stream. If the optical depth is low, then the photons in the ingoing stream are likely to successfully traverse the inner parts of the galaxy and emerge as outgoing photons. In this case,

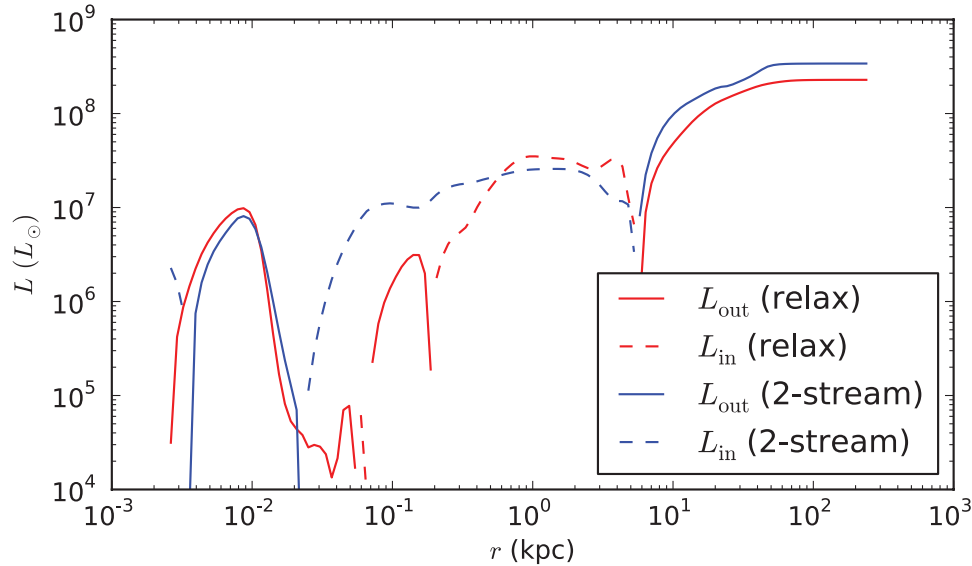


**Figure B1.** The luminosity as a function of radius for the full relaxation based algorithm (Section 3.2) and the simpler two-stream based algorithm (Appendix B). Dashed lines indicate inward-directed luminosities. The solution given by the two-stream approximation described in Appendix B has about 50 per cent more flux at infinity than the ‘true’ solution, and it misses the true solution around 100 pc. However, the solution is quite good given the gains in algorithmic simplicity and reduced computational costs. The function  $\Psi$  associated with  $\zeta = 2$  was used for this figure, where  $\zeta$  is the index of the assumed power-law dependence of photon mean free path on radius used in defining  $\Psi$  (see Appendix B3 for details).

all of the radiation emitted by stars should be considered to be added to the outgoing stream. Doing so gives the correct forces on the material inside and outside the emitting sphere due to the well-known result that for an inverse square force law, there is no net force on a test particle inside a spherical shell of material; and a test particle outside the spherical shell feels a force equal to that of a point source of equivalent mass, charge or luminosity, no matter whether the force is gravitational, electrostatic, or due to momentum transfer by photons.

If the optical depth is large, then the ingoing photons are likely to be absorbed in the inner part of the galaxy. Then only half of the emitted photons should be added to the outgoing stream. The other half should be added to the ingoing stream, where they will in due course be absorbed.

This leads to the following two equations:

$$\frac{dL_{\text{out}}}{dr} = 4\pi r^2 \Psi \dot{E} - \rho \kappa_a L_{\text{out}} \quad (\text{B2})$$

and

$$\frac{dL_{\text{in}}}{dr} = 4\pi r^2 (1 - \Psi) \dot{E} - \rho \kappa_a L_{\text{in}}, \quad (\text{B3})$$

where  $\Psi$  is the fraction of photons emitted at a given radius that are likely to become outgoing photons, either because they were emitted in the outward direction or because they were emitted inwards but are likely to successfully traverse that region without being absorbed. Note that we have defined inward-going luminosities to be negative so that  $L_{\text{in}}$  is negative and  $L = L_{\text{out}} + L_{\text{in}}$ .

## B2 Solving the differential equations

The boundary conditions are  $L_{\text{out}}(r_{\text{min}}) = L_{\text{BH}}$  and  $L_{\text{in}}(r_{\text{max}}) = 0$ , so that equation (B2) is solved by integrating outwards and equation (B3) is solved by integrating inwards.

Summing equations (B2) and (B3) simply gives equation (10), as expected. The advantage of splitting the radiation into an ingoing stream and an outgoing stream is that it transforms a boundary value

problem into an initial value problem, leading to a great reduction of the effort required to find a numerical solution. The quality of the solution will depend on the accuracy of the function  $\Psi$  estimating the contribution that the stars at a given radius make to the ingoing and outgoing streams of radiation. This can of course be checked by comparing to the solution obtained by solving the full boundary value problem.

We have found that this scheme gives reasonable results at a fraction of the algorithmic complexity and computational cost of obtaining the exact solution. Fig. B1 shows the results of solving the radiation transfer equation by the simplified two-stream method and the full solution obtained by solving the boundary value problem for one line of sight in one simulation snapshot. The total optical depth along the line of sight is 13.5. The solution given by the simplified scheme is not perfect, but it is remarkably good given the large optical depth and the reduced algorithmic and computational cost.

## B3 Concerning $\Psi$

If  $p_{\text{abs}}$  is the probability that a given ingoing photon is absorbed before again reaching the radius at which it was emitted (and hence becoming an outgoing photon) and  $p_{\text{trans}} = 1 - p_{\text{abs}}$  is the probability that a given ingoing photon is transmitted so that it again arrives at the radius at which it was emitted and becomes an outgoing photon, then

$$\Psi \equiv 1 - \frac{p_{\text{abs}}}{2} = \frac{1 + p_{\text{trans}}}{2} \quad (\text{B4})$$

The probabilities for absorption and transmission appear in equations (B2) and (B3) only through the quantities  $\Psi$  and  $1 - \Psi$ . Note that of the four ways of writing  $\Psi$  and  $1 - \Psi$  in terms of transmission and absorption probabilities,  $p_{\text{abs}}$  and  $p_{\text{trans}}$  are added to an order-unity constant in all cases except one:  $1 - \Psi = p_{\text{abs}}/2$ . An argument could be made that one should take special care to obtain the correct asymptotic behaviour for  $p_{\text{abs}}$  when  $p_{\text{abs}} \ll 1$  in order to avoid large fractional errors in the ingoing radiation stream. However, this is the optically thin limit, exactly where the ingoing radiation stream

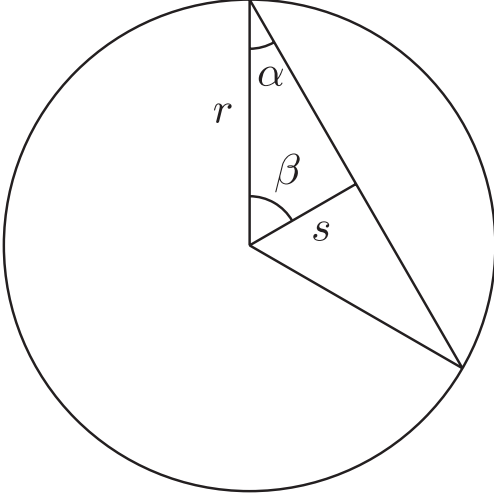


**Figure B2.** Geometry for calculation of optical depth in Section B3.

is expected to be of limited importance. Therefore, any expression for  $\Psi$  with the correct asymptotic limits and a transition between the two limits when the system goes from optically thin to optically thick conditions should introduce only limited fractional errors into equations (B2) and (B3).

The simplest estimate of the fraction of photons emitted at a given radius that are likely to be absorbed at smaller radii comes from finding the apparent size of the sphere where  $\tau = 1$  as seen from the radius  $r$ , where the photons are emitted:

$$\Psi = 1 - \frac{1}{2} \left[ \frac{1}{1 + e^{-\tau}} \right] \left[ \frac{r_1^2}{\max(r_1^2, r^2)} \right], \quad (\text{B5})$$

where  $\tau$  is the optical depth from  $r$  to infinity,  $\tau = \int_r^\infty \rho \kappa dr$ , and  $r_1$  is the radius where the optical depth is unity:  $1 = \int_{r_1}^\infty \rho \kappa dr$ . Here the factor  $1/(1 + e^{-\tau})$  interpolates between the correct asymptotic expressions for the case where  $\tau \ll 1$ ,  $r_1 \ll r$ , in which  $\Psi \simeq 1 - 0.25r_1^2/r^2$  and the case where  $\tau \gg 1$ ,  $r_1 \gg r$  in which  $\Psi \simeq 1/2$ .

More rigorous formulae can be derived assuming spherical symmetry and a power-law dependence of the mean free path for ab-

**Table B1.** Optical depth as a function of photon emission direction in the case of a power-law mean free path, where  $\zeta$  is the power-law index.

$\zeta$	$\tau(\alpha)$
0	$(2r/l_0) \cos \alpha$
1	$(2r/l_0) \log \cot(\alpha/2)$
2	$(r/l_0)(\pi - 2\alpha)/\sin \alpha$
3	$(2r/l_0)\cos \alpha/\sin^2 \alpha$
4	$(r/2l_0)(\pi - 2\alpha + \sin 2\alpha)/\sin^3 \alpha$

sorption on the radius. Given the geometry shown in Fig. B2, the optical depth as a function of the angle  $\alpha$  between the direction of the ray and the line connecting the emission point to the centre of the coordinate system is

$$\tau(\alpha) = \int_0^{\pi-2\alpha} \frac{r \sin \alpha d\beta}{\sin^2(\alpha + \beta) l \left( \frac{r \sin \alpha}{\sin(\alpha + \beta)} \right)}, \quad (\text{B6})$$

where  $r$  is the radius of emission,  $l(s) \equiv 1/\rho(r)\kappa(r)$  is the mean free path to absorption and  $\alpha$ ,  $\beta$  and  $s$  are defined by Fig. B2. The formula gives the optical depth for a photon to traverse the chord of the circle in Fig. B2.

If the mean free path as a function of radius can be approximated by a power law

$$l(s) \approx l_0 \left( \frac{s}{r} \right)^\zeta, \quad \zeta > 0 \quad (\text{B7})$$

where  $l_0$  is the local mean free path at the radius  $r$  at which the photons are emitted, then equation (B6) can be written in terms of hypergeometric functions. However, assuming that  $\zeta$  is an integer gives the simple formulae involving elementary functions given in Table B1.

The transmission probability  $p_{\text{trans}}$  is then

$$p_{\text{trans}} = \int_0^{\pi/2} \sin \alpha e^{-\tau(\alpha)} d\alpha, \quad (\text{B8})$$

so that  $\Psi$  can be recovered from equation (B4).

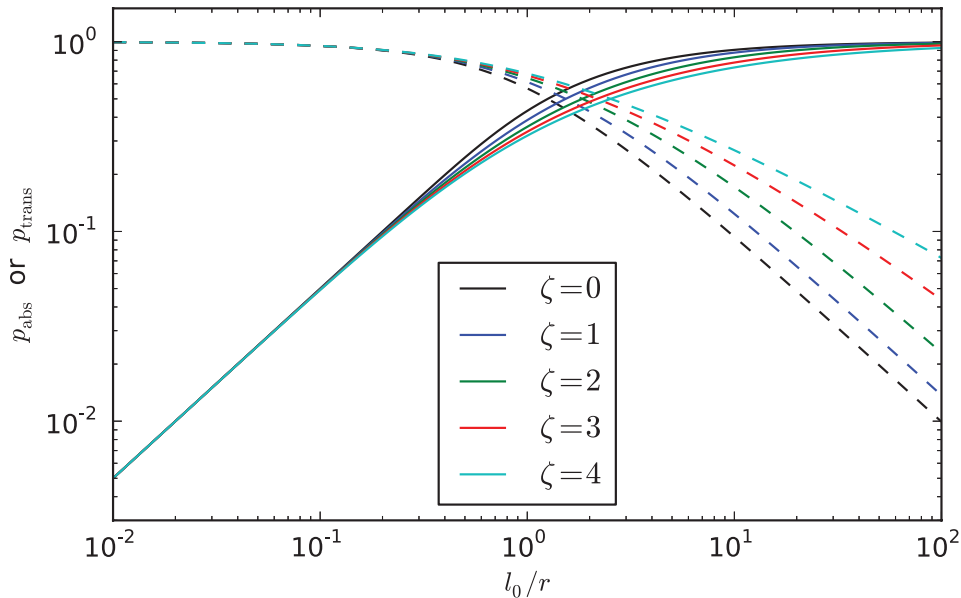


**Figure B3.** Probability of transmission and absorption for spherically symmetric systems with power-law mean free paths of index  $\zeta$ . Solid lines give  $p_{\text{abs}}$ , dashed lines give  $p_{\text{trans}}$ .

The integral in equation (B8) unfortunately cannot be expressed in terms of elementary functions. However, for a given dependence of mean free path on radius, it is a function *only* of the radius in units of the local mean free path  $r/l_0$ . For integral values of  $\zeta$ , the integrand consists of elementary functions, so it can be tabulated at the beginning of a calculation and used throughout with little computational cost. For values of  $\zeta$  from 0 to 4 (corresponding to cases from  $\rho = \text{constant}$  to  $\rho \propto r^{-4}$  if the opacity is constant), the values of  $p_{\text{trans}}$  and  $p_{\text{abs}}$  do not depend sensitively on  $\zeta$ .

Fig. B3 shows  $p_{\text{abs}}$  and  $p_{\text{trans}}$  as a function of optical depth for different values of  $\zeta$ . The precise value of  $\zeta$  makes a moderate difference when the mean free path is roughly equal to the radius of the sphere. In the optically thick limit, the asymptotic form of  $p_{\text{trans}}$  is independent of  $\zeta$  and is given by

$$p_{\text{trans}} \approx 0.005 \left( \frac{l_0}{100r} \right), \quad \text{for } l_0 \ll r. \quad (\text{B9})$$

For the optically thin case, the asymptotic value of  $p_{\text{abs}}$  depends on  $\zeta$ . For values of  $\zeta$  from 0 to 4, the asymptotic form can be

approximated as

$$p_{\text{abs}} \approx \frac{1}{100} \left[ 1 + 6 \left( \frac{\zeta}{4} \right)^2 \right] \left( \frac{\zeta}{4} \right)^{-1+0.4(\zeta/4)^3}, \quad \text{for } l_0 \gg r. \quad (\text{B10})$$

Following the dictum discussed above that errors in  $p_{\text{trans}}$  are tolerable because  $p_{\text{trans}}$  is always added to an order-unity constant, while the same is not true for  $p_{\text{abs}}$  for the ingoing radiation stream when  $p_{\text{abs}}$  is small, one may take the approximation

$$p_{\text{abs}} = \frac{\tilde{p}_{\text{abs}}}{1 + \tilde{p}_{\text{abs}}}, \quad (\text{B11})$$

with  $\tilde{p}_{\text{abs}}$  given by equation (B10) over the whole range of optical depths. The value of  $\Psi$  may then be recovered using equation (B4).

This paper has been typeset from a  $\text{\TeX}/\text{\LaTeX}$  file prepared by the author.